Atmos. Chem. Phys., 25, 14315–14331, 2025
https://doi.org/10.5194/acp-25-14315-2025

Atmospheric Chemistry and Physics
Open Access
EGU

Reaction between linear perfluoroaldehydes and hydroperoxy radical in the atmosphere: reaction mechanisms, reaction kinetics modelling, and atmospheric implications

Zegang Dong[1,2], **Chaolu Xie**[3], **and Bo Long**[1]

[1]School of Materials Science and Engineering, Guizhou Minzu University, Guiyang, 550025, China
[2]School of Chemistry and Chemistry Engineering, South China University of Technology, Guangzhou, 510006, China
[3]College of Physics and Mechatronic Engineering, Guizhou Minzu University, Guiyang, 550025, China

Correspondence: Bo Long (wwwltcommon@sina.com)

Received: 29 December 2024 – Discussion started: 7 March 2025
Revised: 8 August 2025 – Accepted: 7 September 2025 – Published: 3 November 2025

Abstract. Linear perfluoroaldehydes are important products formed in the atmospheric oxidation of industrial fluorinated compounds. However, their atmospheric lifetimes are incompletely known. Here, we employ high level quantum chemistry methods and a dual-level strategy for kinetics to investigate the reactions of C_2F_5CHO and C_3F_7CHO with HO_2. Our calculated results unveil almost equal activation enthalpies at 0 K for linear perfluoroaldehydes reaction with HO_2, indicating that the carbon chain length negligibly influences reaction thermodynamics. The calculated kinetics reveal that vibrational anharmonicity enhances rate constants by a factor of 3–10, while torsional anharmonicity reduces rate constants by 34 %–55 %. Additionally, we also find that the reaction of C_3F_7CHO with HO_2 exhibits significant pressure dependence, with transition pressures ranging from 0.026 to 2.3 bar across a temperature range of 190–350 K. Furthermore, atmospheric lifetimes of C_2F_5CHO and C_3F_7CHO are discussed based on the homogenous and heterogeneous processes. Our findings also reveal that the reactions of C_2F_5CHO and C_3F_7CHO with HO_2 radicals dominate over those with OH radicals in Russia, Malaysia, and parts of Africa by the calculated results in combination with data based on global atmospheric chemical model simulations. Under nighttime conditions, HO_2-initiated degradation represents a major atmospheric sink, comparable in magnitude to photolysis and Cl-initiated oxidation in gas phase, whereas hydrolysis at the air-water interface plays a critical role in the sink of linear perfluoroaldehydes. These findings establish chain-length-dependent pressure effects and conformational sampling as critical, previously unrecognized factors in kinetics calculations, providing a framework for modelling complex fluorotelomer transformations and guiding emission mitigation strategies.

1 Introduction

Poly- and perfluoroalkyl substances (PFASs) are highly fluorinated compounds with long atmospheric lifetimes, which have important influences on global warming potential (GWP) and environmental health (Ackerman Grunfeld et al., 2024; Rupp et al., 2023; Sznajder-Katarzyńska et al., 2019; Wu et al., 2024). During their degradation in the atmosphere, PFASs undergo complex chemical transformations, leading to the formation of linear perfluoroaldehydes. (Alam et al.,2024; Burkholder et al., 2015; David et al., 2021; Wang et al., 2021, 2024). Linear perfluoroaldehydes ($C_nF_{2n+1}CHO$) are significant intermediate compounds, which belong to the aldehydes family of PFASs (Li et al., 2024; Thackray et al., 2020). Chlorofluorocarbons (CFCs) and their temporary replacements, hydrochlorofluorocarbons (HCFCs), hy-

drofluorocarbons (HFCs), and hydrofluoroolefins (HFOs) are the important source of the linear perfluoroaldehydes (Burkholder et al., 2015; Hurley et al., 2006; Martin et al., 2005; Rand and Mabury, 2017; Wang et al., 2023; Waterland and Dobbs, 2007). For example, under low NO_x conditions, the reaction of OH radicals with the potential foaming agent $CF_3(CF_2)_2CH{=}CH_2$ (HFC-1447fz) leads to the formation of C_3F_7CHO (Jiménez et al., 2016; Yu et al., 2024). Furthermore, the atmospheric chemical processes of linear perfluoroaldehydes are of key importance for determining the atmospheric oxidation of fluorotelomer alcohols (FTOHs) (Antiñolo et al., 2012; Hurley et al., 2004).

Linear perfluoroaldehydes were generally considered to be removed through photochemical reactions (Chiappero et al., 2006; Sellevåg et al., 2004) and free radical reactions initiated by OH and Cl radicals (Andersen et al., 2004; Chiappero et al., 2010; Wang et al., 2007). Additionally, NO_3 may also contribute to their atmospheric degradation. (Burkholder et al., 2015; Ziemann and Atkinson, 2012). During the daytime, photolysis of linear perfluoroaldehydes was considered to be the dominant removal process for $C_nF_{2n+1}CHO$, with estimated atmospheric lifetimes ranging from hours to several days (Antiñolo et al., 2014; Chiappero et al., 2006). Antiñolo et al. (2014) reported that the photolysis lifetime of C_2F_5CHO is expected to be 3.5 h at 273 K, with the main degradation products of CF_3CFO and COF_2. In addition, previous investigations have shown that the length of the carbon chain in $C_nF_{2n+1}CHO$ significantly affects the quantum yield of photolysis (Chiappero et al., 2006; Sellevåg et al., 2004). During the nighttime, the reactions of free radicals with $C_nF_{2n+1}CHO$ were considered to be the major degradation pathways. However, previous studies reported relatively slow rate constants for the reaction between OH and $C_nF_{2n+1}CHO$ ($n = 1$–4) with the values of $(6.5\pm1.2)\times10^{-13}$, $(5.57\pm0.07)\times10^{-13}$, $(5.8\pm0.6)\times10^{-13}$, and $(6.1\pm0.5)\times10^{-13}$ cm^3 molecule^{-1} s^{-1}, respectively, at 298 K (Andersen et al., 2004; Antiñolo et al., 2014; Solignac et al., 2007). This corresponds to a longer atmospheric lifetime > 20 d for these linear perfluoroaldehydes. Moreover, the rate constant of Cl atoms with $C_nF_{2n+1}CHO$ ($n = 1$–4) is approximately 2×10^{12} cm^3 molecule^{-1} s^{-1}. This value is slightly faster than that of the corresponding OH radical reactions under similar conditions (Andersen et al., 2004; Sulbaek Andersen et al., 2003). The long atmospheric lifetimes of $C_nF_{2n+1}CHO$ provide an opportunity for other atmospheric oxidation processes of $C_nF_{2n+1}CHO$ by other atmospheric oxidants.

HO_2 radicalsare of ubiquitous active species in the atmosphere with the concentration being two orders of magnitude higher than that of OH radicals (Bottorff et al., 2023; Gao et al., 2024; Albrecht et al., 2019; Zhang et al., 2019, 2024, 2022) . Moreover, previous investigations have shown that the reactions of aldehydes with HO_2 affect the degradation process of aldehydes (Hermans et al., 2005; Albrecht et al., 2019; Zhou et al., 2024a). Additionally, global three-dimensional chemistry-transport model calculations suggest that the oxidation reactions of formaldehyde and acetone initiated by hydroperoxyl radical contribute to 30 % loss of formaldehyde and acetone at the tropical troposphere (Hermans et al., 2005). Nevertheless, the importance of sink pathway by HO_2 is still unknown because there have not been kinetics data for linear perfluoroaldehydes with HO_2 in the literature. Moreover, chain elongation may have influences on reaction kinetics due to multiple conformers. Furthermore, it is unknown for the pressure-dependent effects of larger perfluoroaldehydes with HO_2. Although our previous investigations have revealed the importance of $CF_3CHO + HO_2$ in the atmosphere (Long et al., 2022), their kinetics of larger perfluoroaldehydes with HO_2 are further required to investigate due to the unique features that depend on the specific reaction systems such as multi-structural anharmonicity and pressure effects in these complex systems. Additionally, it is a big challenge for addressing the larger perfluoroaldehydes with HO_2 because the computational cost grows very rapidly with system size, making such calculations impractical for high-level quantum chemistry methods.

In this article, we have investigated the reactions of HO_2 with linear perfluoroaldehydes $C_nF_{2n+1}CHO$ ($n = 2$–5), specifically focusing on C_2F_5CHO and C_3F_7CHO, referred to as Reactions (R1) and (R2) respectively. To delve into these reactions, high-level quantum chemistry calculation close to CCSDT(Q) accuracy in conjunction with dual-level strategy were performed to obtain their quantitative kinetics. Simultaneously, to provide further insight into kinetics, we detailly evaluated the impact of various parameters, including torsional anharmonicity, anharmonicity on the reaction kinetics over atmosphere-related temperatures and pressures. In addition, the chemical transformation of the formed intermediate products has been discussed in Reactions (R1) and (R2). We further estimate the enthalpies of activation at 0 K for the larger-sized reactions of longer-chain perfluoroaldehyde with HO_2. Moreover, we also discuss the importance of these Reactions (R1) and (R2) by combining the calculated reaction kinetics with global atmospheric modelling. The current results not only provide a comparative analysis with the kinetics of analogous OH-initiated reactions and photolytic processes, but also extend our understanding of the role of HO_2 in modulating the atmospheric lifetime of linear perfluoroaldehydes. This study not only resolves the knowledge gap regarding HO_2-initiated oxidation of linear perfluoroaldehydes but also establishes a computational strategy for predicting the atmospheric fates of long-chain PFAS derivatives. Our findings provide critical insights for refining emission control strategies and mitigating the environmental persistence of these compounds.

$$C_2F_5CHO + HO_2 \rightarrow C_2F_5CH(OH)OO \quad \text{(R1)}$$

$$C_3F_7CHO + HO_2 \rightarrow C_3F_7CH(OH)OO \quad \text{(R2)}$$

2 Computational methods and atmospheric modelling

2.1 Options for electronic structure density functionals

Our goal is to establish a precise set of electronic structure and kinetic calculation methods for the $XCHO + HO_2$ reaction, delivering satisfactory quantitative results (Long et al., 2022). This previous study indicated that the CCSD(T)-F12a/cc-pVTZ-F12//M06-2X/MG3S theoretical methods can make good agreement with beyond-CCSD(T) results for the similar reaction of $HCHO + HO_2$ (Long et al., 2022). Furthermore, CCSD(T)-F12a/cc-pVTZ-F12 has been shown good performance for molecules containing fluorine atoms (Dong et al., 2021; Long et al., 2022; Xia et al., 2024a). Consequently, we intend to utilize the well-validated methods in the present investigations in Reactions (R1) and (R2). Specifically, the M06-2X (Zhao and Truhlar, 2008b, a) density functional with the MG3S (Lynch et al., 2003) basis set was employed to optimize the geometries, while CCSD(T)-F12a (Adler et al., 2007; Knizia et al., 2009)/cc-pVTZ-F12 for R1 and R2 and FNO-CCSD(T)-F12 (Gyevi-Nagy et al., 2021; Taube and Bartlett, 2008)/cc-pVDZ-F12 for other $C_nF_{2n+1}CHO + HO_2$ ($n = 1$–5) were used to calculate single-point energies. The FNO-CCSD(T) approach that significantly improves computational efficiency with cost reduction of up to an order of magnitude was utilized to calculate larger systems. Furthermore, intrinsic reaction coordinate (IRC) calculation was done to determine the correct transition states by examining the connections of each saddle point to its corresponding minima (Hratchian and Schlegel, 2004, 2005; Kenyon, 1968).

2.2 Vibrational frequencies

We found that standard scale factor is actually not applicable for some transition states in previous investigation, so we used two scale factors (Zheng et al., 2014, 2015). The standard scale factor for M06-2X/MG3S is 0.970. Furthermore, we also calculated the specific reaction scale factors to assess the effects of anharmonicity. The reaction-specific scale factors were obtained by using the MPW1K/6-311+G(2df, 2p) electronic structure method based on the hybrid degeneracy-corrected second-order vibrational perturbation theory (HD-CVPT) (Bloino et al., 2012; Kuhler et al., 1996). This is necessary and effective for eliminating the activation enthalpy error caused by the standard scale factors and the results were listed in Tables S1 and S2 in the Supplement. This was obtained by Eq. (1),

$$\lambda^{\mathrm{SRP,ZPE}} = \lambda^{\mathrm{Anh}}\lambda^{\mathrm{H}} \quad (1)$$

where λ^{Anh} is the ratio of anharmonic zero-point vibrational energies (ZPE) to harmonic ZPE at the MPW1K/6-311+G(2df, 2p) level. λ^{H} is 0.983 for M06-2X/MG3S to correct harmonic frequencies. The result shows that the specific reaction scale factors are 0.955 for TS1 (see Table S1) and 0.956 for TS2 (see Table S1), which is a large deviation from the standard value of 0.970; this results in a decrease in calculated enthalpies of activation of 0.72 and 0.78 for TS1 and TS2 at 0 K, respectively. In addition, multi-structural torsional anharmonicity involving reactant and transition state were all calculated using MS-T method (multi-structural method for torsional anharmonicity) (Yu et al., 2012; Zheng et al., 2011; Zheng and Truhlar, 2013).

2.3 Kinetics calculations

The dual-level strategy was utilized to compute the high-pressure limit rate constant (Long et al., 2016, 2019; Xia et al., 2024a). As shown in Eq. (2), we integrated a conventional transition-state theory rate constant $k_{\mathrm{TST}}^{\mathrm{HL}}$ predicated on higher-level (HL, CCSD(T)-F12a/cc-pVTZ-F12//M06-2X/MG3S) inputs with transmission coefficients derived from direct dynamics at a lower level (LL, M11-L/MG3S), employing a specific density functional that is chosen from the results of benchmark calculations (see Table S3). We have incorporated both a recrossing transmission coefficient $k_{\mathrm{CVT/TST}}^{\mathrm{LL}}$ and a tunneling transmission coefficient $k_{\mathrm{SCT}}^{\mathrm{LL}}$, as calculated through reaction-path variational transition state theory, with a particular emphasis on the canonical variational theory coupled with small-curvature tunneling (CVT/SCT) (Garrett and Truhlar, 1979; Liu et al., 1993; Truhlar et al., 1982). Additionally, a multi-structural transmission coefficient ($F^{\mathrm{MS\text{-}T}}$) was introduced to this framework to cancel the errors caused by the multi-structural anharmonicity, thereby advancing our approach to the DL-MS-CVT/SCT method, which provides a detailed and multifaceted treatment of the rate constant calculation, and can effectively obtain quantitative kinetics.

$$k_{\mathrm{MS\text{-}CVT/SCT}}^{\mathrm{DL}} = F^{\mathrm{MS\text{-}T}} \times k_{\mathrm{TST}}^{\mathrm{HL}} \times k_{\mathrm{SCT}}^{\mathrm{LL}} \times \Gamma_{\mathrm{CVT/TST}}^{\mathrm{LL}} \quad (2)$$

The pressure-dependent rate constants were done by employing the system-specific quantum Rice-Ramsperger-Kassel (SS-QRRK) theory in the temperature range of 190–350 K (Bao et al., 2016a, b; Bao and Truhlar, 2017). This method relies only on the high-pressure limiting rate constant that was calculated by the dual-level strategy. The computational details of pressure-dependent rate constants are presented in the Supplement.

2.4 Atmospheric modelling

We used GEOS-Chem 14.4.2 with a horizontal resolution of $2.0° \times 2.5°$ to simulate space distribution of HO_2 and OH at 47 vertical layers in the period from February 2018 to February 2019 (Bey et al., 2001). The time includes six months of spin-up and output per hour. GEOS-Chem is a global, three-dimensional chemical transport model associated with atmospheric composition (http://geos-chem.org, last access: 16 October 2025). Modern-Era Retrospective

analysis for Research and Applications, Version 2 (MERRA-2) (Gelaro et al., 2017) was used as meteorological field data and Harmonized Emissions Component (HEMCO 3.9) was used as the source of emissions data (Lin et al., 2021). The emissions include biogenic emissions from Model of Emissions of Gases and Aerosols from Nature (MEGANv2.1) (Hu et al., 2015; McDuffie et al., 2020) and anthropogenic emissions from the global Community Emissions Data System (CEDS) (McDuffie et al., 2020) inventory. Simulation uses default full chemistry mechanism including HO_x-NO_x-VOC-O_3-halogen chemistry, which is done by our previous investigation (Bloss et al., 2007).

2.5 Software

All density function calculation, including Zero-point energy (ZPE) correction were carried out using Gaussian 16 software package (Zhao and Truhlar, 2008b) and the single point energy calculations for CCSD(T)-F12a/cc-pVTZ-F12 and FNO-CCSD(T)-F12a/cc-pVDZ-F12 were done using Molpro 2019 (Werner et al., 2019) and MRCC code (Kállay et al., 2020, 2022). MS-T method was executed through MSTor-2023 program package (Chen et al., 2023). The rate constants were done with the KiSThelP (Canneaux et al., 2014) Polyrate 2017-C (Zheng et al., 2017) and Gaussrate 2017-B (Zheng et al., 2018).

3 Results and discussion

3.1 The electronic structure of the $C_2F_5CHO/C_3F_7CHO + HO_2$ reaction

We considered the $C_2F_5CHO/C_3F_7CHO + HO_2$ reaction similar to the reactions of aldehydes with HO_2 (Long et al., 2022). The dominant mechanism is that the hydrogen atom of HO_2 is transferred to the terminal oxygen atom of C_2F_5CHO/C_3F_7CHO, and simultaneously, the oxygen atom of HO_2 is connected to the carbon atom of carbonyl group of C_2F_5CHO/C_3F_7CHO. Figure 1 depicts ZPE corrected potential energy profile of the reaction of $C_2F_5CHO/C_3F_7CHO + HO_2$ at the CCSD(T)-F12a/cc-pVTZ-F12//M06-2X/MG3S level. C_2F_5CHO/C_3F_7CHO and HO_2 form reaction complexes RC1/RC2, and then pass through transition states TS1 and TS2 to form the intermediate products of $C_2F_5CH(OH)OO$ (M1) and $C_3F_7CH(OH)OO$ (M2), respectively. TS1 ($-2.7\,kcal\,mol^{-1}$) denotes the global minimum optimized structures of the stationary points of enthalpy of activation at 0 K; this is 0.3 and $1.6\,kcal\,mol^{-1}$ lower than that of the $CF_3CHO + HO_2$ and $CH_3CHO + HO_2$ reactions, respectively (Long et al., 2022). This shows that the reaction of perfluoroaldehydes with HO_2 may be kinetically feasible. As a comparison, the further energy profile of the $C_3H_7CHO + HO_2$ reaction shows an equal enthalpy of activation of $-2.7\,kcal\,mol^{-1}$ for TS2; this is slightly lower than that of enthalpy of activation $-2.4\,kcal\,mol^{-1}$ for the reaction of $CF_3CHO + HO_2$ (Gao et al., 2024).

It is noteworthy that Fig. 1 only depicts the potential energy profile of the reaction featuring the global minimum structure. Nevertheless, the internal rotation of the C–C bond produces multiple conformers for reactants, transition states, and formed intermediate products. Their geometric configurations and energy distributions relative to the global minimum structure are presented in Fig. S1. Regarding the reactions of C_2H_5CHO and C_3H_7CHO with HO_2, we have observed that as the carbon chain lengthens, the number of conformers of both reactants and transition states increases, and the energy distribution broadens. For instance, TS1 has three isomers, with an energy distribution spanning from 0 to $1.7\,kcal\,mol^{-1}$, whereas TS2 has five isomers, and its energy distribution ranges from 0 to $1.9\,kcal\,mol^{-1}$. In terms of geometric configurations, the low-energy isomers tend to have more linear structures, while the high-energy conformations exhibit more pronounced curling.

NO is a highly reactive gas (Lee et al., 2024). Human activities, especially agriculture and industrial processes, have led to significant NO emissions (Andersen et al., 2024; Thomson et al., 2012). Industrial activities contribute to NO levels such as fossil fuel combustion in power plants and chemical manufacturing, along with vehicle emissions. Given its prevalence from human-induced emissions, we further explore the degradation pathways of intermediate products M1 and M2 in the presence of NO. As depicted in Fig. S2, M1 and M2 undergo initial reactions with NO to yield the products $C_2F_5CH(O)OH$, $C_3F_7CH(O)OH$, and NO_2, exhibiting activation enthalpies of -9.9 and $-11.5\,kcal\,mol^{-1}$ at 0 K, respectively. These results are consistent with previous studies on similar reactions involving RO_2+ NO. (Berndt et al., 2015; King et al., 2001; Nie et al., 2023; Orlando et al., 2000; Vereecken and Peeters, 2009). These products then undergo unimolecular reactions to decompose into C_2F_5 and C_3F_7 radicals and formic acid in Fig. 2. Notably, the unimolecular decomposition of $C_2F_5CH(O)OH$ and $C_3F_7CH(O)OH$ represents the rate-determining step of the overall reaction, with corresponding activation enthalpies of 5.6 and $4.7\,kcal\,mol^{-1}$ (0 K), respectively; this indicates that formic acid may potentially be formed via $C_2F_5CHO/C_3F_7CHO + HO_2$ in the presence of high concentration NO in the atmosphere. Additionally, the formed intermediate products (M1 and M2) are a typical class of RO_2 radicals. In the low NO_x levels, these RO_2 radicals can also participate in bimolecular reactions (Ding and Long, 2022). RO_2 can react with HO_2, resulting in the formation of the stable product ROOH. Moreover, RO_2 can react with other RO2 or $R'O_2$ (where R′ denotes a hydrocarbon fragment) (Bottorff et al., 2023). The reaction with $R'O_2$ frequently yields alkoxy radicals, and both of these reactions are capable of producing stable products (Goldman et al., 2021). Due to the complexity of these bimolecular reactions of the formed RO_2 in the Reactions (R1)

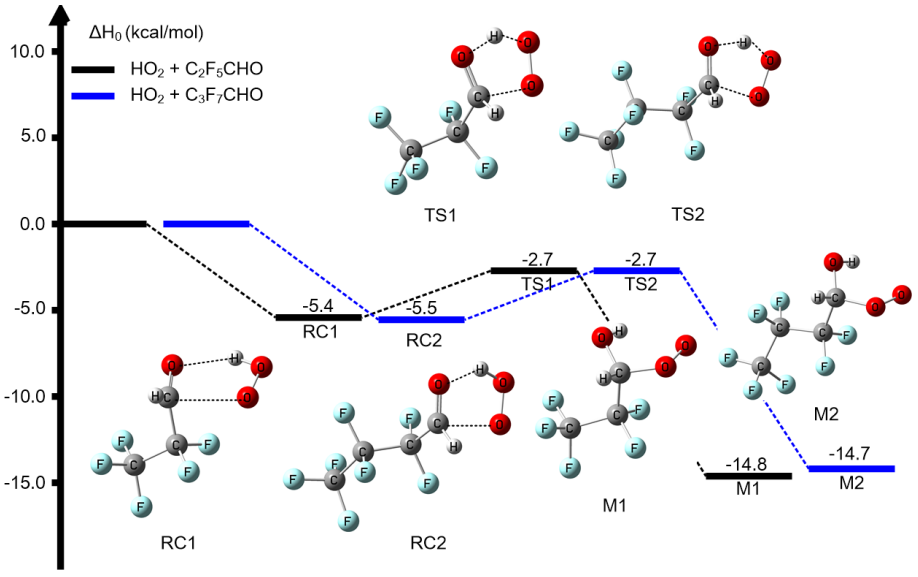

Figure 1. Enthalpy profile of the HO_2 addition reaction with C_2F_5CHO and C_3F_7CHO as calculated by CCSD(T)-F12a/cc-pVTZ-F12//M06-2X/MG3S level with the scale factor by the standard method at 0 K.

and (R2), we did not further investigate their reaction mechanisms and kinetics in the present work.

We further conducted an extended study on the reactions of C_4F_9CHO and $C_5F_{11}CHO$ at the FNO-CCSD(T)-F12//cc-pVDZ-F12//M06-2X/MG3S level, aiming to investigate the effects of increasing carbon chain length on the enthalpy of activation at 0 K. The calculated results show a deviation of only 0.2 kcal mol^{-1} in activation enthalpy at 0 K between FNO-CCSD(T)-F12//cc-pVDZ-F12 (-2.6 kcal mol^{-1}) and CCSD(T)-F12a/cc-pVTZ-F12 (-2.4 kcal mol^{-1}) in $CF_3CHO + HO_2$, validating the robustness of FNO-CCSD(T)-F12//cc-pVDZ-F12 for complex fluorinated systems. Data from Fig. 3 reveal an interesting phenomenon that the activation enthalpy at 0 K remains almost equal C_2 (C_2F_5CHO) to C_5 ($C_5F_{11}CHO$). This finding aligns with the similar trend for the reaction of $C_nH_{2n+1}CHO$ with HO_2, suggesting that the impact of carbon chain length growth on the enthalpy of activation at 0 K is quite minor (Ding and Long, 2022; Gao et al., 2024). However, the introduction of CF_3 leads to a relatively lower enthalpy of activation at 0 K for the $C_nH_{2n+1}CHO + HO_2$ reactions, primarily due to the strong electron-withdrawing ability of fluorine atoms, which can stabilize the transition state and lower the enthalpy of activation at 0 K. As the size of perfluoroaldehyde increases, the multi-structure effects caused by torsion of C-C bonds become more pronounced. The relative energy values of reactants and transition states shown in Figs. S1 and S3 (relative to the global minimum energy value, without ZPE correction) indicate that with increasing molecular size, the number of possible isomers increases, leading to a broader energy distribution. For instance, C_2F_5CHO exhibits three transition state conformers with energy differences spanning 0–1.7 kcal mol^{-1}, while C_3F_7CHO has five conformers distributed over 0–1.8 kcal mol^{-1}. This trend amplifies for longer chains: $C_5F_{11}CHO$ generates 36 distinct conformers in its transition state, with energy variations extending up to 4.8 kcal mol^{-1}. This broad energy distribution has significant implications for the thermodynamics and kinetics of the degradation process of perfluoroaldehydes, potentially increasing the diversity and complexity of reaction pathways.

3.2 Kinetics of $C_2F_5CHO/C_3F_7CHO + HO_2$

The high-pressure limiting rate constants were calculated for the temperature range of 190-350 K, covering a wide atmospheric temperature range. For the reactions $C_2F_5CHO + HO_2$ (Reaction R1) and $C_3F_7CHO + HO_2$ (Reaction R2), the rate constants incorporating multi-structure anharmonicity corrections are defined as k_1 andk_2, respectively. According to Zheng and Truhlar (2010), the rate constants at high pressure are fitted using Eq. (3).

$$k = A\left(\frac{T+T_0}{300}\right)^n \exp\left[-\frac{E\,(T+T_0)}{R\left(T^2+T_0^2\right)}\right] \tag{3}$$

Table S4 lists the fitting parameters A, n, E, and T_0. Here, T represents temperature in Kelvin, and R is the ideal gas constant (0.0019872 kcal mol^{-1} K^{-1}). The temperature-dependent Arrhenius activation energies are determined from the fits using Eq. (4).

$$E_0 = -R\frac{\mathrm{d}lnk}{\mathrm{d}(1/T)} \tag{4}$$

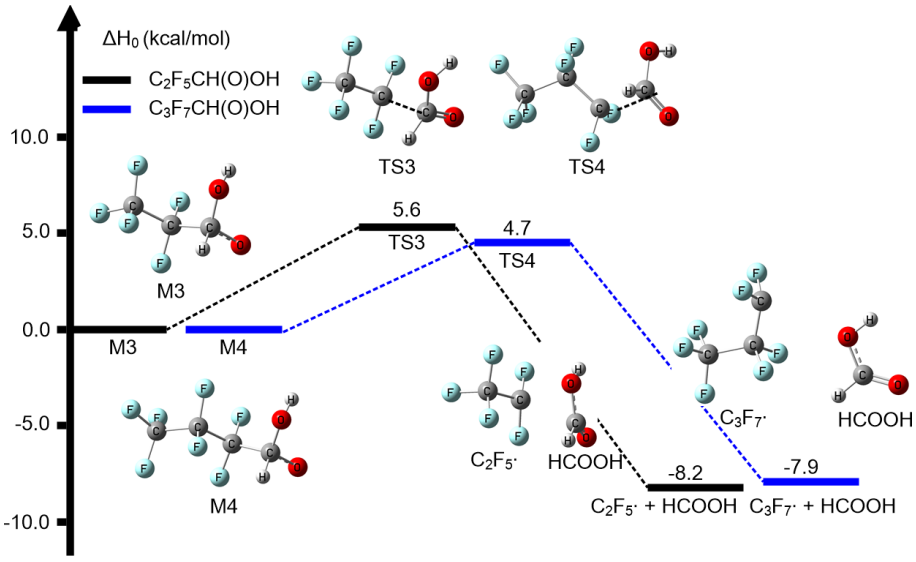

Figure 2. Relative enthalpies at 0 K for the decomposition of $C_2F_5CH(O)OH$ (M3) and $C_3F_7CH(O)OH$ (M4) calculated by CCSD(T)-F12a/cc-pVTZ-F12//M06-2X/MG3S.

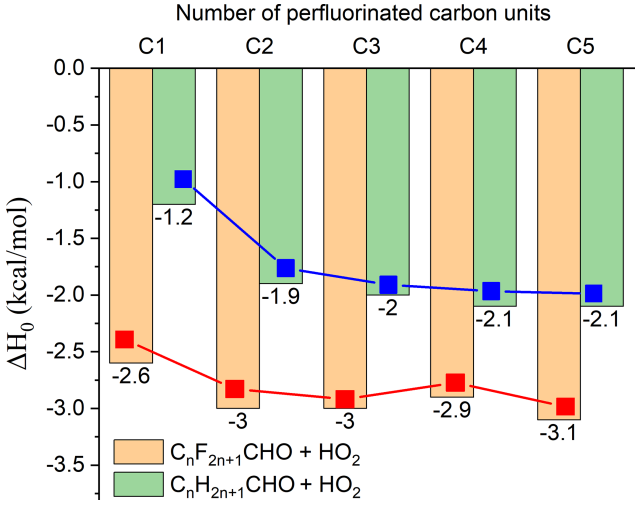

Figure 3. The impacts of perfluorinated carbon length on the enthalpies of activation at 0 K in the $C_nH_{2n+1}CHO/C_nF_{2n+1}CHO + HO_2$ reactions. The values for $C_nH_{2n+1}CHO$ (n = 1–5) + HO_2 and $C_nF_{2n+1}CHO + HO_2$ are obtained from references (Ding and Long, 2022; Gao et al., 2024) and calculated by using FNO-CCSD(T)-F12a/cc-pVDZ-F12.

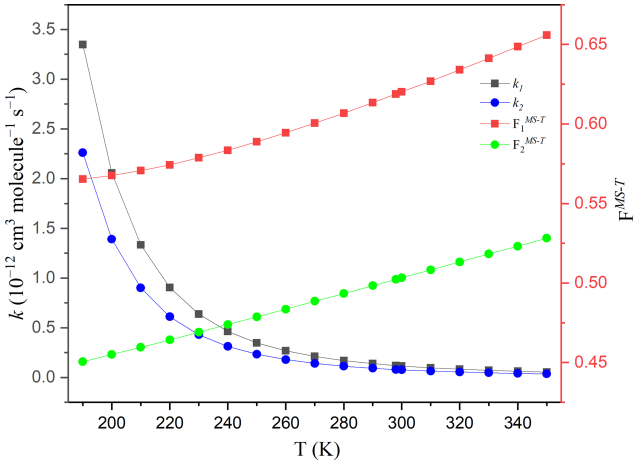

Figure 4. The high-pressure limit rate constants of the reactions of C_2F_5CHO and C_3F_7CHO with HO_2 at the temperature range of 190–350 K.

The high-pressure limit rate constants, incorporating multiple-structure anharmonicity torsional corrections, are illustrated in Fig. 4, with more comprehensive data provided in Tables S5–S7. Regarding the $C_2F_5CHO + HO_2$ reaction, the rate constant k_1 exhibits a decrease from 3.35×10^{-12} cm^3 molecule^{-1} s^{-1} at 190 K to 5.42×10^{-14} cm^3 molecule^{-1} s^{-1} at 350 K in Fig. 4 and Tables S5–S7. Similarly, the rate constant k_2 for the $C_3F_7CHO + HO_2$ reaction also decreases with increasing temperature. These trends are consistent with theoretical studies of non-fluorinated aldehydes such as C_2H_5CHO and C_3H_7CHO, where rate constants for reactions with HO_2 were reported in the range of 10^{-14} to 10^{-13} cm^3 molecule^{-1} s^{-1} at atmospheric temperatures, indicating similar reactivity between fluorinated and non-fluorinated aldehydes with HO_2 (Ding and Long, 2022; Gao et al., 2024).

In addition, the effects of recrossing and multi-structural anharmonicity are quite limited, approximately ranging between 0.4 and 0.7 times. This results in the rate constants for Reactions (R1) and (R2) being 2–3 times slower than that of $CF_3CHO + HO_2$. For instance, the rate constants of $C_2F_5CHO + HO_2$ and $C_3F_7CHO + HO_2$ are estimated

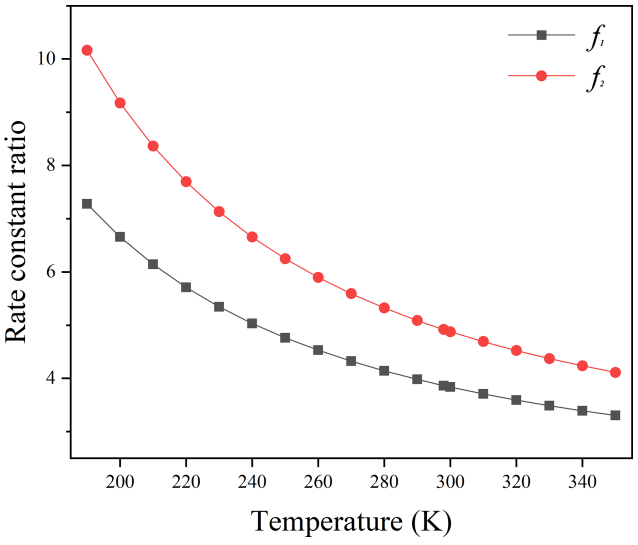

Figure 5. The ratio between the rate constant calculated using the reaction-specific vibrational-frequency scale factors and the rate constant calculated using the standard vibrational-frequency scale factors, within the temperature range of 190–350 K. f_1 and f_2 represent the ratios for the reactions of $C_2F_5CHO + HO_2$ and $C_3F_7CHO + HO_2$, respectively.

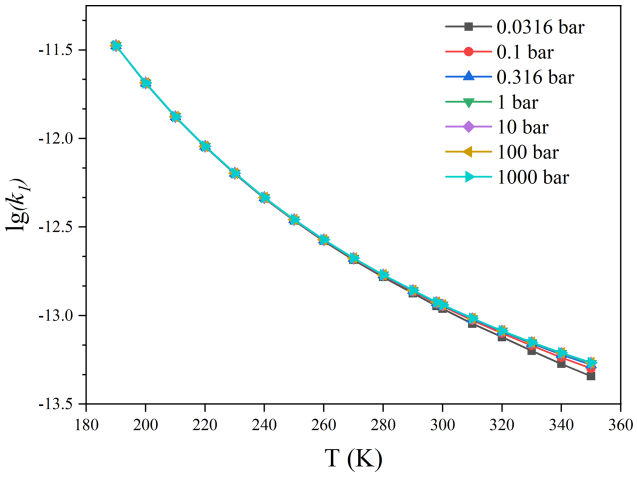

Figure 6. Pressure-dependent rate constants of $C_2F_5CHO + HO_2$ as functions of temperature obtained via the SS-QRRK method.

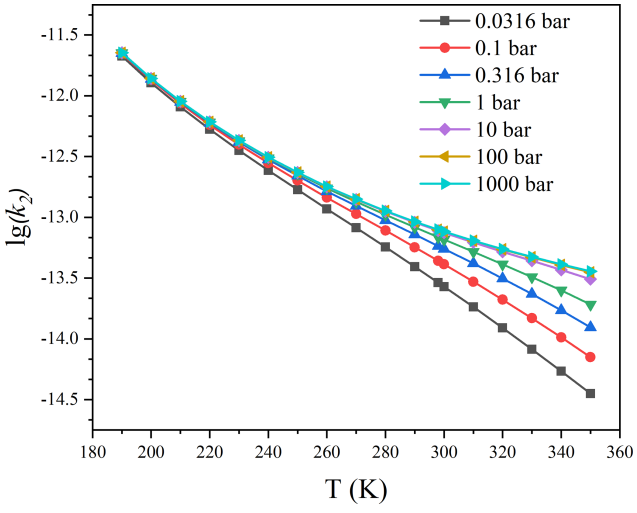

Figure 7. Pressure-dependent rate constants of $C_3F_7CHO + HO_2$ as functions of temperature obtained via the SS-QRRK method.

to be 1.19×10^{-13} and 7.92×10^{-14} cm^3 molecule^{-1} s^{-1} at 298 K, respectively, which is slow by compared to 2.48×10^{-13} cm^3 molecule^{-1} s^{-1} of $CF_3CHO + HO_2$ (Long et al., 2022). Moreover, the effect of anharmonicity in vibrational-frequency scale factors on high pressure limited rate constants were further discussed. We define "f" as the ratio between the rate constant calculated using the reaction-specific vibrational-frequency scale factors and that calculated using the standard vibrational-frequency scale factors. As depicted in Fig. 5, the rate constants obtained using the reaction-specific scale factors are 3–7 and 4–10 times faster compared to those calculated using the standard scale factors. Consequently, employing reaction-specific scale factors is crucial for accurate rate calculations.

The pressure-dependent rate constants of the HO_2 reaction with C_2F_5CHO and C_3F_7CHO were further calculated by using SS-QRRK method. As shown in Figs. 6–7 and Tables S8–S9, it can be observed that variations of the calculated rate constant with respect to pressure have a minimal impact on the rate constant of $C_2F_5CHO + HO_2$, indicating the absence of significant pressure effects. However, significant pressure effects are observed in the $C_3F_7CHO + HO_2$ reaction, particularly at temperatures above 300 K. To provide a clearer perspective, we define the transition pressure $p_{1/2}$ to quantify the pressure dependence. Specifically, the transition pressure $p_{1/2}$ is the pressure at which the pressure-dependent rate constant reaches half of its high-pressure limit. Figure 8 and Table S10 show that the transition pressure $p_{1/2}$ for the $HO_2 + C_2F_5CHO$ reaction ranging from 2.6×10^{-5} to 7.4×10^{-3} bar at 190–350 K, while the transition pressure $p_{1/2}$ ranges from 2.6×10^{-2} to 2.3 bar at 190–350 K for the $HO_2 + C_3F_7CHO$ reaction. This indicates that the $HO_2 + C_3F_7CHO$ reaction exhibits a significant pressure dependence, and the increase in carbon chain length has a significantly affect pressure-dependent rate constants.

3.3 Atmospheric Implications

To provide a further insight into the atmospheric degradation pathways of linear perfluoroaldehydes, we compare the HO_2-initiated linear perfluoroaldehyde reactions with the corresponding reactions with OH and Cl atom, their photolysis and hydrolysis.

We quantitatively evaluate the relative importance of OH- versus HO_2-initiated degradation for C_2F_5CHO and

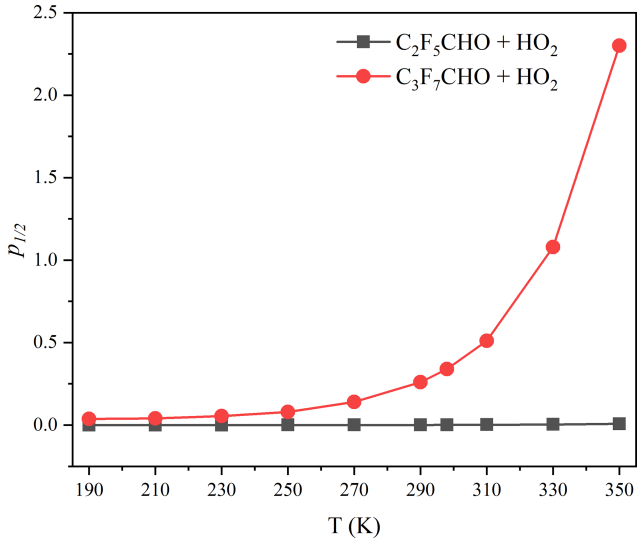

Figure 8. Transition pressure $p_{1/2}$ calculated by the SS-QRRK method for the $HO_2 + C_2F_5CHO$ and $HO_2 + C_3F_7CHO$ reactions as functions of temperature.

C_3F_7CHO through rate ratios defined in Eqs. (5) and (6).

$$v_1 = \frac{k_1 [C_2F_5CHO][HO_2]}{k_{OH}[C_2F_5CHO][OH]} \quad (5)$$

$$v_2 = \frac{k_2 [C_3F_7CHO][HO_2]}{k_{OH'}[C_3F_7CHO][OH]} \quad (6)$$

Here, k_1 and k_2 are the rate constants of $HO_2 + C_2F_5CHO$ and $HO_2 + C_3F_7CHO$ calculated in the present work, respectively, while k_{OH} and $k_{OH'}$ are the corresponding rate constants of $OH + C_2F_5CHO$ and $OH + C_3F_7CHO$ obtained in the literature (Solignac et al., 2007; Wang et al., 2007). We calculate the rate ratios using a high OH concentration of 5×10^6 molecules cm^{-3} (Lew et al., 2020) and a typical HO_2 concentration of 1.4×10^8 molecules cm^{-3} (Brasseur and Solomon, 2006). The calculated results reveal that within the temperature range of 220–320 K, the rate ratios for v_1 and v_2 are in the range of 79.2 to 3.76 and 45.7 to 2.43, respectively (Table 1). Therefore, the present findings indicate that HO_2 initiated reactions dominate over OH initiated reactions for the degradation of C_2F_5CHO and C_3F_7CHO. We further consider the atmospheric lifetimes of C_2F_5CHO and C_3F_7CHO with respect to HO_2 at 0–50 km altitude in Table 2. Rapid HO_2-initiated degradation leads to short atmospheric lifetimes of ~ 14.4–31.3 h for C_2F_5CHO and 21.6–51.8 h for C_3F_7CHO (Table 2), which are significantly shorter than the ~ 20 d atmospheric lifetime driven by OH oxidation at below 10 km (Antiñolo et al., 2014).

To provide further insight into the degradation of C_2F_5CHO and C_3F_7CHO under atmospheric conditions, further analysis has been done based on Geos-Chem data. GEOS-Chem simulations indicate that HO_2 concentrations reach a maximum of 4.99×10^8 molecules cm^{-3} in the Amazon region, with a mean value of 9.93×10^7 molecules cm^{-3} (Long et al., 2024). In contrast, the maximum OH concentration over the Atlantic and Pacific oceans is found to be 8.03×10^6 molecules cm^{-3}, with an average value of 1.06×10^6 molecules cm^{-3}. (Lelieveld et al., 2016). However, the OH concentration remarkably differ from daytime to nighttime (Bey et al., 1997; Stone et al., 2012). Therefore, we consider the concentration ratio between HO_2 and OH during the nighttime and daytime. During the nighttime, as shown in Fig. 9, the concentration ratio of $[HO_2]/[OH]$ exceeds two orders of magnitude in industrial regions such as Russia, Malaysia, and parts of Africa, with values reaching as high as 410–1200 in the Amazon. This markedly enhances the HO_2-to-OH degradation rate ratios for C_2F_5CHO and C_3F_7CHO, reaching values of 88.5–259 and 56.0–164, respectively. This suggest that HO_2-initiated degradation exceeds OH-initiated pathways by more than a factor of 50 during nighttime in these regions. In contrast, over oceanic regions such as the Atlantic and Pacific, the $[HO_2]/[OH]$ ratio falls below unity, substantially reducing the contribution of HO_2 to degradation processes in these areas.

During the nighttime, as shown in Fig. S4, the concentration ratios between HO_2 and OH generally favor HO_2, exhibiting maxima up to three orders of magnitude along the western coast of South America and ranging from one to two orders of magnitude in industrialized and African regions. These elevated ratios are closely associated with localized emission sources. However, During the daytime, photolysis is also an important route for removal of C_2F_5CHO and C_3F_7CHO. For C_2F_5CHO and C_3F_7CHO, photolysis represents the dominant atmospheric degradation route. C_2F_5CHO exhibits a high photolysis quantum yield of 0.81 ± 0.09 at 254 nm, corresponding to an estimated atmospheric lifetime of less than 2 d in Table 3. Similarly, C_3F_7CHO displays a measured photolysis lifetime of 21 ± 10 h under sunlight, confirming the efficiency of this removal mechanism (Chiappero et al., 2006; Solignac et al., 2007).

Table 1. Rate ratios of $HO_2 + C_2F_5CHO$ to $OH + C_2F_5CHO$ and $HO_2 + C_3F_7CHO$ to $OH + C_3F_7CHO$ within the Temperature Range of 240 to 350 K.

T (K)	k_1 [a]	k_2' [a]	v_1 [b]	v_2 [b]
220	9.04×10^{-13}	6.10×10^{-13}	79.2	45.7
240	4.64×10^{-13}	3.12×10^{-13}	34.22	20.34
260	2.68×10^{-13}	1.79×10^{-13}	17.09	10.38
280	1.70×10^{-13}	1.13×10^{-13}	9.55	5.90
298	1.19×10^{-13}	7.92×10^{-13}	6.06	3.83
320	8.21×10^{-13}	5.48×10^{-13}	3.76	2.43

[a] k_1 and k_2' are the rate constants of the HO_2 reactions with C_2F_5CHO and C_3F_7CHO, from the literature respectively. [b] v_1 and v_2 denote the rate ratios of HO_2 with C_2F_5CHO and C_3F_7CHO to OH with C_2F_5CHO and C_3F_7CHO, respectively.

Table 2. Hydroperoxyl radical concentration (in molecules cm^{-3}), rate constants (in cm^3 molecule^{-1} s^{-1}), and atmospheric lifetimes (in hours) with respect to bimolecular reactions as functions of altitude.

H (km)[a]	T (K)[a]	P (mbar)[a]	$[HO_2]$[b]	k_1 (T, p)[c]	k_2 (T, p)[c]	τ_1^d	τ_2^d
0	290.2	1010	1.40×10^8	1.38×10^{-13}	9.18×10^{-14}	14.4	21.6
5	250.5	496	4.90×10^7	3.44×10^{-13}	2.30×10^{-13}	16.5	24.7
10	215.6	243	8.30×10^6	1.07×10^{-12}	6.47×10^{-13}	31.3	51.8
15	198	119	2.30×10^6	2.21×10^{-12}	2.98×10^{-13}	54.7	4.05×10^2
20	208	58.2	2.90×10^6	1.38×10^{-12}	1.22×10^{-13}	69.3	7.85×10^2
25	216.1	28.5	5.70×10^6	9.38×10^{-13}	4.32×10^{-14}	52.0	1.13×10^3
30	221.5	13.9	7.50×10^6	6.52×10^{-13}	1.29×10^{-14}	56.8	2.88×10^3
35	228.1	6.83	6.90×10^6	4.04×10^{-13}	4.13×10^{-15}	99.6	9.74×10^3
40	240.5	3.34	5.90×10^6	2.29×10^{-13}	1.73×10^{-15}	2.06×10^2	2.73×10^4
45	251.9	1.64	4.90×10^6	1.27×10^{-13}	6.56×10^{-16}	4.45×10^2	8.64×10^4
50	253.7	0.801	4.00×10^6	5.87×10^{-13}	1.80×10^{-16}	1.18×10^3	3.86×10^5

[a] H denotes altitude (atmospheric scale height); T denotes temperature; p denotes pressure. [b] Data are from Brasseur and Solomon (2006). [c] k_1, k_2 are the rate constants of the HO_2 reactions with C_2F_5CHO and C_3F_7CHO, respectively. [d] $\tau_1 = 1/(k[HO_2])$ and $\tau_2 = 1/(k_2[HO_2])$ define the atmospheric lifetimes for HO_2 reactions with C_2F_5CHO and C_3F_7CHO, respectively.

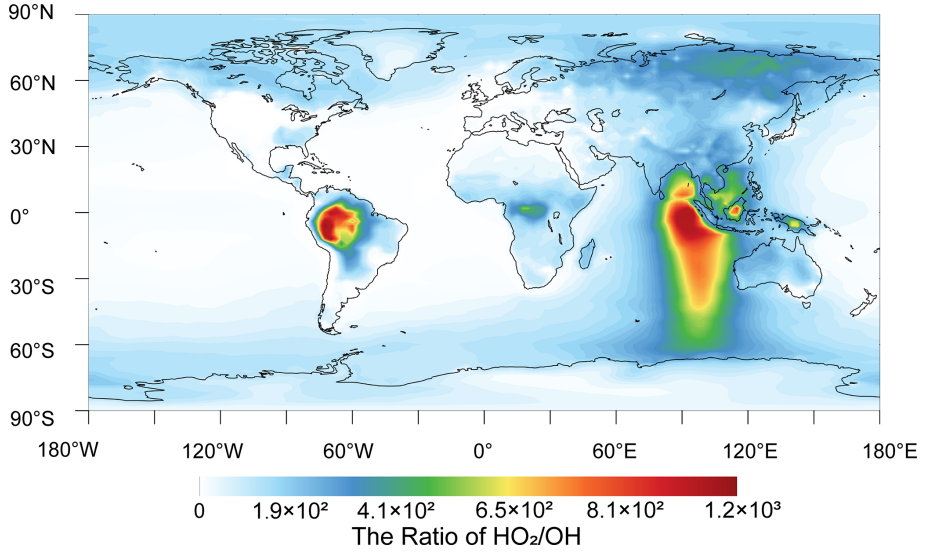

Figure 9. The annual average ratio of HO_2/OH at night globally.

Chlorine atom reactions represent an additional potential atmospheric degradation pathway for linear perfluoroaldehydes. Kinetic measurements report rate constants of $k(Cl + C_2F_5CHO) = (1.96 \pm 0.28) \times 10^{-12}$ cm^3 molecule^{-1} s^{-1} (Sulbaek Andersen et al., 2003) and $k(Cl + C_3F_7CHO) = (2.03 \pm 0.23) \times 10^{-12}$ cm^3 molecule^{-1} s^{-1} (Andersen et al., 2004), which are approximately one order of magnitude higher than those for the corresponding HO_2-initiated reactions. Although Cl atoms exhibit intrinsically faster reaction kinetics, the atmospheric relevance of this degradation pathway is limited by the relatively low concentrations of Cl in the troposphere. Typical Cl atom concentrations range from 1.0×10^4 to 3.0×10^5 molecules cm^{-3} (Chang et al., 2004; Hossaini et al., 2016; Wang et al., 2019), leading to estimated atmospheric lifetimes of approximately 400 h ($\sim$ 17 d) for both C_2F_5CHO and C_3F_7CHO. This stands in sharp contrast to the significantly shorter HO_2-driven lifetimes, which are typically less than 79.2 h in the lower troposphere in Table 3. The predominance of HO_2-mediated degradation arises from the relatively high ambient concentrations of HO_2, which compensate for its slower reaction kinetics – particularly in regions such as the Amazon, where $[HO_2]/[Cl]$ ratios may exceed $\sim 10^3$ (Li et al., 2018; Wang et al., 2019). Under such conditions, the HO_2 initiated reaction rate can exceed that of Cl by 2–3 orders of magnitude. Moreover, the

Table 3. Atmospheric lifetimes (τ, hours) of C_2F_5CHO and C_3F_7CHO against major degradation pathways.

Reactant/Process	C_2F_5CHO		C_3F_7CHO	
	τ (hours)	Ref.	τ (hours)	Ref.
HO_2	3.76–79.2	This work	2.43–45.7	This work
OH	90.8–174.2	Antiñolo et al. (2014)	79.7–113.0	Solignac et al. (2007)
Photolysis	< 48	Chiappero et al. (2006)	14.6–39.7	Solignac et al. (2007)
Cl	424.4–571.6	Sulbaek Andersen et al. (2003)	409.7–514.4	Andersen et al. (2004)
Hydrolysis[a]	$> 5.39 \times 10^6$	This work	–	–
HCOOH catalysis[b]	$> 5.06 \times 10^7$	This work	$> 1.13 \times 10^8$	This work
Heterogeneous hydrolysis[c]	3.47×10^{-4}	This work	–	–

[a] Gas-phase hydrolysis of C_2F_5CHO with H_2O. [b] HCOOH-catalyzed gas-phase hydrolysis of C_2F_5CHO/C_3F_7CHO with H_2O. [c] Hydrolysis of C_2F_5CHO with water dimer at the air-water interface.

atmospheric relevance of Cl-initiated degradation is further constrained by its spatial heterogeneity, being primarily restricted to marine boundary layers and polluted coastal environments (Hossaini et al., 2016; Yang et al., 2022). In contrast, HO_2-driven degradation is effective across continental interiors and industrialized regions.

In addition to photolysis and radical-initiated oxidation, hydrolysis constitutes another potential atmospheric sink for C_2F_5CHO and C_3F_7CHO. Taking C_2F_5CHO hydrolysis as an example, its gas phase hydrolysis proceeds extremely slowly, with an estimated atmospheric lifetime exceeding 5.39×10^6 h (Tables 3 and S11). This removal pathway is negligible, aligning with findings reported for CF_3CHO (Sulbaek Andersen et al., 2006). Hydrolysis catalyzed by atmospheric acids could potentially enhance hydrolysis rates through its ability to reduce the reaction barriers (Hazra et al., 2013; Liu et al., 2021). Formic acid (HCOOH), a ubiquitous atmospheric component, forms stable complexes with water ($HCOOH\cdots H_2O$). Even at elevated concentrations of $HCOOH\cdots H_2O$ complexes (e.g., 10^{11} molecule cm^{-3}), the estimated hydrolysis lifetimes of C_2F_5CHO and C_3F_7CHO exceed 10^7 h in Table 3. These timescales remain orders of magnitude longer than those associated with HO_2-initiated degradation, suggesting that the acid-catalyzed hydrolysis is insufficient to promote significant atmospheric removal of these compounds. Therefore, although acid catalysis effectively reduces the reaction barrier, its impact on the gas-phase degradation of C_2F_5CHO and C_3F_7CHO is negligible under typical tropospheric conditions.

Hydrolysis at air–water interfaces, such as those present on aerosol particles and cloud droplets, proceeds with markedly enhanced efficiency. Laboratory experiments have shown that passing gaseous CF_3CHO through liquid water results in over 80 % conversion to $CF_3CH(OH)_2$ within seconds, highlighting the potential importance of heterogeneous processes in atmospheric removal pathways (Sulbaek Andersen et al., 2006). Similarly, ^1H NMR measurements reveal that C_2F_5CHO rapidly converts to its gem-diol form, $CF_3CF_2CH(OH)_2$, within 3 min upon contact with liquid water, further confirming the efficient aqueous-phase hydration of perfluoroaldehydes. (Sulbaek Andersen et al., 2006). Here, we estimate a low Gibbs free-energy barrier ($\Delta G = 9.8$ kcal mol^{-1}) for $C_2F_5CHO + 3H_2O$ at air-water interfaces, proceeding via a cyclic proton-transfer mechanism by using ab initio molecular dynamics, compared to a much higher barrier of 25.5 kcal mol^{-1} for the corresponding gas-phase reaction (see Fig. S5a, b). More details are provided in Supplement. This results in significantly shorter atmospheric lifetimes, on the order of 3.47×10^{-4} h. Under humid conditions, such air–water interfacial hydrolysis is likely to dominate and may effectively compete with HO_2-mediated degradation pathways. Once formed, $C_nF_{2n+1}CH(OH)_2$ reacts with OH, ultimately leading to the formation of perfluorocarboxylic acids (PFCAs). This hydrolysis-oxidation pathway represents a significant indirect source of persistent PFCAs, particularly given the ubiquity of aqueous phases in the atmosphere.

We can conclude that HO_2 initiated degradation pathways dominate the gas-phase degradation of C_2F_5CHO and C_3F_7CHO. We further consider the final product in the $HO_2 + C_nF_{2n+1}CHO$ reactions. As mentioned, the HO_2 reaction generates intermediate perfluoroalkyl radicals C_nF_{2n+1}, which can subsequently undergo a carbon-shortening process to form the more stable COF_2, as depicted in Fig. 10. Taking the example of C_2F_5, the process starts with C_2F_5 reacting with O_2 to form $C_2F_5O_2$. Subsequently, $C_2F_5O_2$ reacts with NO to produce C_2F_5O, which then undergoes C-C bond cleavage to generate CF_3 and COF_2. The CF_3 further reacts to eventually yield COF_2 through a similar reaction pathway. However, the absence of quantified rate constants for these reactions prevents a robust assessment of their global or regional impacts. A comprehensive evaluation of the role of NO would require integrating the kinetics of $RO_2 + NO$ reactions (e.g., M1/M2+NO) into atmospheric models, which is beyond the scope of this study.

In summary, we identify that the HO_2-initiated reaction represents an important atmospheric sink for linear perfluoroaldehydes in gas phase. Notably, recent studies suggest that

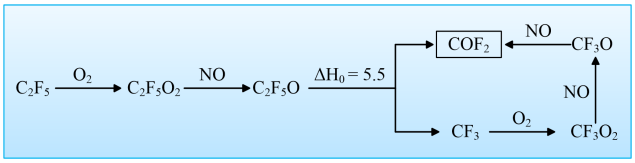

Figure 10. Atmospheric degradation mechanism for C_nF_{2n+1} with C_2F_5 used as a representative example.

HO_2 concentrations may be elevated at air–water interfaces compared to the bulk gas phase (Angelaki et al., 2024; Li et al., 2023). Given the enhanced reactivity at the air–water interface and the complex competition between OH and HO_2, interfacial HO_2-driven degradation may play a more significant role than previously recognized, potentially influencing atmospheric acidity. For example, Xia et al. (2024b) recently reported both single-carbon and double-carbon scission pathways during the degradation of C_7F_{15} on water droplet surfaces. These heterogeneous processes may contribute not only to the atmospheric removal of perfluoroaldehydes but also to the broader degradation of polyfluoroalkyl substances (PFAS). Nevertheless, further experimental and theoretical studies on reaction kinetics and mechanisms are needed to better constrain this complex chemical processes. Incorporating such processes into atmospheric models is crucial for improving the prediction of PFAS environmental fate and secondary pollution, with important implications for emission control strategies and environmental risk assessment.

4 Summarizing Remarks

In this study, we have delved into the chemical reaction kinetics of linear perfluoroaldehydes (C_2F_5CHO and C_3F_7CHO) with hydroperoxyl radicals in the gas phase using ab initio calculation methods and reaction kinetics theory. We find that the activation enthalpies for the reactions of C_2F_5CHO and C_3F_7CHO with HO_2 at 0 K are both $-2.7\,kcal\,mol^{-1}$, demonstrating that carbon chain elongation in linear perfluoroaldehydes has a negligible thermodynamic influence on their enthalpies of activation at 0 K. This is further shown in C_4F_9CHO and $C_5F_{11}CHO$ with HO_2.

Further kinetic studies reveal that anharmonicity have a significant impact on the reaction rates, while the torsional anharmonicity, recross coefficient, and tunnelling effects contribute relatively little to the rate constants. It is particularly noteworthy that the reaction of C_3F_7CHO with HO_2 exhibits a distinct pressure dependence, whereas the reaction of C_2F_5CHO with HO_2 does not show such a pressure effect.

By integrating kinetics with the data based on GEOS-Chem modelling, we have identified some regions such as Russia, Malaysia, and parts of Africa, where HO_2 concentration exceeds OH concentration by 2–3 orders of magnitude. Therefore, the reactions of HO_2 with C_2F_5CHO and C_3F_7CHO can compete well with their corresponding reaction with OH. Specifically, the atmospheric lifetimes of C_2F_5CHO and C_3F_7CHO via HO_2 are shortened to be 14.4–31.3 and 21.6–51.8 h, respectively, with orders of magnitude shorter than that of the corresponding OH-mediated pathways. In addition, photolysis, typically occurring within 48 h, represents an efficient daytime removal pathway, while heterogeneous hydrolysis proceeds rapidly at air-water interfaces with characteristic timescales of less than 1 h. Accordingly, HO_2-initiated degradation should be considered a major gas-phase sink, particularly in continental source regions. Under high NO_x conditions, this pathway may contribute to tropospheric HCOOH and COF2 formation.

While the present investigation establishes the HO_2-mediated degradation pathway for linear perfluoroaldehydes (C_2F_5CHO/C_3F_7CHO), it simultaneously highlights critical gaps in our understanding of their atmospheric lifetimes. Notably, the current work focuses on gas-phase HO_2 reactions. However, the roles of heterogeneous interfacial processes (e.g., on aerosol surfaces or cloud droplets) remain unexplored (Zhang et al., 2024). The potential for HO_2-driven defluorination to generate reactive CF_3 radicals, which could initiate secondary reactions (e.g., with O_3 or NO_2), requires systematic investigation to assess implications for atmospheric oxidizing capacity and secondary aerosol formation. Additionally, the study focuses on radical-driven pathways but acknowledges that photolysis is a competing sink for linear perfluoroaldehydes. Future work should quantify photolysis rates under stratospheric UV conditions (e.g., 200–300 nm) to reconcile discrepancies between modeled and observed atmospheric lifetimes (Thomson et al., 2025). Addressing these limitations will require integrating advanced experimental techniques (e.g., synchrotron-based photoionization mass spectrometry) with multi-scale modeling frameworks, while prioritizing under sampled environments like the upper troposphere and polar regions where HO_2 reactivity anomalies could profoundly alter PFAS degradation trajectories (Alam et al., 2024; Zhou et al., 2024b). Such efforts are critical for refining environmental risk assessments of emerging HFOs and guiding the design of next-generation chemicals with minimized atmospheric persistence.

Data availability. All data from this research can be obtained upon request by contacting Bo Long (wwwltcommon@sina.com) or Zegang Dong (dzegang@sina.com).

Supplement. The supplement related to this article is available online at https://doi.org/10.5194/acp-25-14315-2025-supplement.

Author contributions. BL designed the project; ZD performed the quantum chemical calculations; CX performed the model calculations; ZD, CX, and BL analysed the data; ZD wrote the

manuscript draft. ZD, CX, and BL reviewed and edited the manuscript.

Competing interests. The contact author has declared that none of the authors has any competing interests.

Disclaimer. Publisher's note: Copernicus Publications remains neutral with regard to jurisdictional claims made in the text, published maps, institutional affiliations, or any other geographical representation in this paper. While Copernicus Publications makes every effort to include appropriate place names, the final responsibility lies with the authors. Also, please note that this paper has not received English language copy-editing. Views expressed in the text are those of the authors and do not necessarily reflect the views of the publisher.

Financial support. This work was supported in part by the National Natural Science Foundation of China (grant nos. 42120104007 and 41775125) and by Guizhou Provincial Science and Technology Projects, China (grant nos. ZK [2022]194, CXTD [2022]001, and GCC [2023]026).

Review statement. This paper was edited by Zhibin Wang and reviewed by three anonymous referees.

References

Ackerman Grunfeld, D., Gilbert, D., Hou, J., Jones, A. M., Lee, M. J., Kibbey, T. C. G., and O'Carroll, D. M.: Underestimated burden of per- and polyfluoroalkyl substances in global surface waters and groundwaters, Nature Geoscience, 17, 340–346, https://doi.org/10.1038/s41561-024-01402-8, 2024.

Adler, T. B., Knizia, G., and Werner, H. J.: A simple and efficient CCSD(T)-F12 approximation, Journal of Chemical Physics, 127, 221106, https://doi.org/10.1063/1.2817618, 2007.

Alam, M. S., Abbasi, A., and Chen, G.: Fate, distribution, and transport dynamics of Per- and Polyfluoroalkyl Substances (PFASs) in the environment, Journal of Environmental Management, 371, 123163, https://doi.org/10.1016/j.jenvman.2024.123163, 2024.

Albrecht, S. R., Novelli, A., Hofzumahaus, A., Kang, S., Baker, Y., Mentel, T., Wahner, A., and Fuchs, H.: Measurements of hydroperoxy radicals (HO_2) at atmospheric concentrations using bromide chemical ionisation mass spectrometry, Atmos. Meas. Tech., 12, 891–902, https://doi.org/10.5194/amt-12-891-2019, 2019.

Andersen, M. P. S., Nielsen, O. J., Hurley, M. D., Ball, J. C., Wallington, T. J., Stevens, J. E., Martin, J. W., Ellis, D. A., and Mabury, S. A.: Atmospheric chemistry of n-$C_xF_{2x+1}CHO$ ($x = 1, 3, 4$): Reaction with Cl atoms, OH radicals and IR spectra of $C_xF_{2x+1}C(O)O_2NO_2$, Journal of Physical Chemistry A, 108, 5189–5196, https://doi.org/10.1021/jp0496598, 2004.

Andersen, S. T., McGillen, M. R., Xue, C., Seubert, T., Dewald, P., Türk, G. N. T. E., Schuladen, J., Denjean, C., Etienne, J.-C., Garrouste, O., Jamar, M., Harb, S., Cirtog, M., Michoud, V., Cazaunau, M., Bergé, A., Cantrell, C., Dusanter, S., Picquet-Varrault, B., Kukui, A., Mellouki, A., Carpenter, L. J., Lelieveld, J., and Crowley, J. N.: Measurement report: Sources, sinks, and lifetime of NO_x in a suburban temperate forest at night, Atmos. Chem. Phys., 24, 11603–11618, https://doi.org/10.5194/acp-24-11603-2024, 2024.

Angelaki, M., Carreira Mendes Da Silva, Y., Perrier, S., and George, C.: Quantification and Mechanistic Investigation of the Spontaneous H_2O_2 Generation at the Interfaces of Salt-Containing Aqueous Droplets, Journal of the American Chemical Society, 146, 8327–8334, https://doi.org/10.1021/jacs.3c14040, 2024.

Antiñolo, M., González, S., Ballesteros, B., Albaladejo, J., and Jiménez, E.: Laboratory studies of $CHF_2CF_2CH_2OH$ and $CF_3CF_2CH_2OH$: UV and IR absorption cross sections and OH rate coefficients between 263 and 358 K, Journal of Physical Chemistry A, 116, 6041–6050, https://doi.org/10.1021/jp2111633, 2012.

Antiñolo, M., Jiménez, E., González, S., and Albaladejo, J.: Atmospheric chemistry of CF_3CF_2CHO: Absorption cross sections in the UV and IR regions, photolysis at 308 nm, and gas-phase reaction with OH radicals ($T = 263$–358 K), Journal of Physical Chemistry A, 118, 178–186, https://doi.org/10.1021/jp410283v, 2014.

Bao, J. L. and Truhlar, D. G.: Variational transition state theory: Theoretical framework and recent developments, Chemical Society Reviews, 46, 7548–7596, https://doi.org/10.1039/c7cs00602k, 2017.

Bao, J. L., Zhang, X., and Truhlar, D. G.: Predicting pressure-dependent unimolecular rate constants using variational transition state theory with multidimensional tunneling combined with system-specific quantum RRK theory: A definitive test for fluoroform dissociation, Physical Chemistry Chemical Physics, 18, 16659–16670, https://doi.org/10.1039/c6cp02765b, 2016a.

Bao, J. L., Zheng, J., and Truhlar, D. G.: Kinetics of Hydrogen Radical Reactions with Toluene Including Chemical Activation Theory Employing System-Specific Quantum RRK Theory Calibrated by Variational Transition State Theory, Journal of the American Chemical Society, 138, 2690–2704, https://doi.org/10.1021/jacs.5b11938, 2016b.

Berndt, T., Richters, S., Kaethner, R., Voigtländer, J., Stratmann, F., Sipilä, M., Kulmala, M., and Herrmann, H.: Gas-Phase Ozonolysis of Cycloalkenes: Formation of Highly Oxidized RO_2 Radicals and Their Reactions with NO, NO_2, SO_2, and Other RO_2 Radicals, Journal of Physical Chemistry A, 119, 10336–10348, https://doi.org/10.1021/acs.jpca.5b07295, 2015.

Bey, I., Aumont, B., and Toupance, G.: The nighttime production of OH radicals in the continental troposphere, Geophysical Research Letters, 24, 1067–1070, https://doi.org/10.1029/97GL00889, 1997.

Bey, I., Jacob, D. J., Yantosca, R. M., Logan, J. A., Field, B. D., Fiore, A. M., Li, Q., Liu, H. Y., Mickley, L. J., and Schultz, M. G.: Global modeling of tropospheric chemistry with assimilated meteorology: Model description and evaluation, Journal of Geophysical Research-Atmospheres, 106, 23073–23095, https://doi.org/10.1029/2001JD000807, 2001.

Bloino, J., Biczysko, M., and Barone, V.: General perturbative approach for spectroscopy, thermodynamics, and kinetics: Methodological background and benchmark studies, Jour-

nal of Chemical Theory and Computation, 8, 1015–1036, https://doi.org/10.1021/ct200814m, 2012.

Bloss, W. J., Lee, J. D., Heard, D. E., Salmon, R. A., Bauguitte, S. J.-B., Roscoe, H. K., and Jones, A. E.: Observations of OH and HO_2 radicals in coastal Antarctica, Atmos. Chem. Phys., 7, 4171–4185, https://doi.org/10.5194/acp-7-4171-2007, 2007.

Bottorff, B., Lew, M. M., Woo, Y., Rickly, P., Rollings, M. D., Deming, B., Anderson, D. C., Wood, E., Alwe, H. D., Millet, D. B., Weinheimer, A., Tyndall, G., Ortega, J., Dusanter, S., Leonardis, T., Flynn, J., Erickson, M., Alvarez, S., Rivera-Rios, J. C., Shutter, J. D., Keutsch, F., Helmig, D., Wang, W., Allen, H. M., Slade, J. H., Shepson, P. B., Bertman, S., and Stevens, P. S.: OH, HO_2, and RO_2 radical chemistry in a rural forest environment: measurements, model comparisons, and evidence of a missing radical sink, Atmos. Chem. Phys., 23, 10287–10311, https://doi.org/10.5194/acp-23-10287-2023, 2023.

Brasseur, G. and Solomon, S.: Aeronomy of the middle atmosphere: chemistry and physics of the stratosphere and mesosphere, Springer Science & Business Media, 617–627 pp., https://doi.org/10.1007/1-4020-3824-0, 2006.

Burkholder, J. B., Cox, R. A., and Ravishankara, A. R.: Atmospheric Degradation of Ozone Depleting Substances, Their Substitutes, and Related Species, Chemical Reviews, 115, 3704–3759, https://doi.org/10.1021/cr5006759, 2015.

Canneaux, S., Bohr, F., and Henon, E.: KiSThelP: A program to predict thermodynamic properties and rate constants from quantum chemistry results, Journal of Computational Chemistry, 35, 82–93, https://doi.org/10.1002/jcc.23470, 2014.

Chang, C. T., Liu, T. H., and Jeng, F. T.: Atmospheric concentrations of the Cl atom, CIO radical, and HO radical in the coastal marine boundary layer, Environmental Research, 94, 67–74, https://doi.org/10.1016/j.envres.2003.07.008, 2004.

Chen, W., Zheng, J., Bao, J. L., Truhlar, D. G., and Xu, X.: MSTor 2023: A new version of the computer code for multistructural torsional anharmonicity, now with automatic torsional identification using redundant internal coordinates, Computer Physics Communications, 288, 108740, https://doi.org/10.1016/j.cpc.2023.108740, 2023.

Chiappero, M. S., Malanca, F. E., Argüello, G. A., Wooldridge, S. T., Hurley, M. D., Ball, J. C., Wallington, T. J., Waterland, R. L., and Buck, R. C.: Atmospheric chemistry of perfluoroaldehydes ($C_xF_{2x+1}CHO$) and fluorotelomer aldehydes ($C_xF_{2x+1}CH_2CHO$): Quantification of the important role, of photolysis, Journal of Physical Chemistry A, 110, 11944–11953, https://doi.org/10.1021/jp064262k, 2006.

Chiappero, M. S., Argüello, G. A., Hurley, M. D., and Wallington, T. J.: Atmospheric chemistry of n-$C_6F_{13}CH_2CHO$: Formation from n-$C_6F_{13}CH_2CH_2OH$, kinetics, and mechanisms of reactions with chlorine atoms and OH radicals, Journal of Physical Chemistry A, 114, 6131–6137, https://doi.org/10.1021/jp101587m, 2010.

David, L. M., Barth, M., Höglund-Isaksson, L., Purohit, P., Velders, G. J. M., Glaser, S., and Ravishankara, A. R.: Trifluoroacetic acid deposition from emissions of HFO-1234yf in India, China, and the Middle East, Atmos. Chem. Phys., 21, 14833–14849, doi10.5194/acp-21-14833-2021, 2021.

Ding, D. P. and Long, B.: Reaction between propionaldehyde and hydroxyperoxy radical in the atmosphere: A reaction route for the sink of propionaldehyde and the formation of formic acid, Atmospheric Environment, 284, 119202, https://doi.org/10.1016/j.atmosenv.2022.119202, 2022.

Dong, Z. G., Xu, F., Mitchell, E., and Long, B.: Trifluoroacetaldehyde aminolysis catalyzed by a single water molecule: An important sink pathway for trifluoroacetaldehyde and a potential pathway for secondary organic aerosol growth, Atmospheric Environment, 249, 118242, https://doi.org/10.1016/j.atmosenv.2021.118242, 2021.

Gao, Q., Shen, C., Zhang, H., Long, B., and Truhlar, D. G.: Quantitative Kinetics Reveal that Reactions of HO_2 are a Significant Sink for Aldehydes in the Atmosphere and may Initiate the Formation of Highly Oxygenated Molecules via Autoxidation , Physical Chemistry Chemical Physics, 26, 16160–16174, https://doi.org/10.1039/d4cp00693c, 2024.

Garrett, B. C. and Truhlar, D. G.: Criterion of minimum state density in the transition state theory of bimolecular reactions, The Journal of Chemical Physics, 70, 1593–1598, https://doi.org/10.1063/1.437698, 1979.

Gelaro, R., McCarty, W., Suárez, M. J., Todling, R., Molod, A., Takacs, L., Randles, C. A., Darmenov, A., Bosilovich, M. G., Reichle, R., Wargan, K., Coy, L., Cullather, R., Draper, C., Akella, S., Buchard, V., Conaty, A., da Silva, A. M., Gu, W., Kim, G. K., Koster, R., Lucchesi, R., Merkova, D., Nielsen, J. E., Partyka, G., Pawson, S., Putman, W., Rienecker, M., Schubert, S. D., Sienkiewicz, M., and Zhao, B.: The modern-era retrospective analysis for research and applications, version 2 (MERRA-2), Journal of Climate, 30, 5419–5454, https://doi.org/10.1175/JCLI-D-16-0758.1, 2017.

Goldman, M. J., Green, W. H., and Kroll, J. H.: Chemistry of Simple Organic Peroxy Radicals under Atmospheric through Combustion Conditions: Role of Temperature, Pressure, and NO_x Level, Journal of Physical Chemistry A, 125, 10303–10314, https://doi.org/10.1021/acs.jpca.1c07203, 2021.

Gyevi-Nagy, L., Kállay, M., and Nagy, P. R.: Accurate Reduced-Cost CCSD(T) Energies: Parallel Implementation, Benchmarks, and Large-Scale Applications, Journal of Chemical Theory and Computation, 17, 860–878, https://doi.org/10.1021/acs.jctc.0c01077, 2021.

Hazra, M. K., Francisco, J. S., and Sinha, A.: Gas phase hydrolysis of formaldehyde to form methanediol: Impact of formic acid catalysis, Journal of Physical Chemistry A, 117, 11704–11710, https://doi.org/10.1021/jp4008043, 2013.

Hermans, I., Müller, J. F., Nguyen, T. L., Jacobs, P. A., and Peeters, J.: Kinetics of α-Hydroxy-alkylperoxyl radicals in oxidation processes. HO_2?-Initiated oxidation of ketones/aldehydes near the tropopause, Journal of Physical Chemistry A, 109, 4303–4311, https://doi.org/10.1021/jp044080v, 2005.

Hossaini, R., Chipperfield, M. P., Saiz-Lopez, A., Fernandez, R., Monks, S., Feng, W., Brauer, P., and Von Glasow, R.: A global model of tropospheric chlorine chemistry: Organic versus inorganic sources and impact on methane oxidation, Journal of Geophysical Research, 121, 14271–14297, https://doi.org/10.1002/2016JD025756, 2016.

Hratchian, H. P. and Schlegel, H. B.: Accurate reaction paths using a Hessian based predictor-corrector integrator, Journal of Chemical Physics, 120, 9918–9924, https://doi.org/10.1063/1.1724823, 2004.

Hratchian, H. P. and Schlegel, H. B.: Using Hessian Updating To Increase the Efficiency of a Hessian Based Predictor-Corrector

Reaction Path Following Method, Journal of Chemical Theory and Computation, 1, 61–69, 2005.

Hu, L., Millet, D. B., Baasandorj, M., Griffis, T. J., Turner, P., Helmig, D., Curtis, A. J., and Hueber, J.: Isoprene emissions and impacts over an ecological transition region in the U.S. Upper Midwest inferred from tall tower measurements, Journal of Geophysical Research-Atmospheres, 120, 3553–3571, https://doi.org/10.1002/2014JD022732, 2015.

Hurley, M. D., Wallington, T. J., Sulbaek Andersen, M. P., Ellis, D. A., Martin, J. W., and Mabury, S. A.: Atmospheric chemistry of fluorinated alcohols: Reaction with Cl atoms and OH radicals and atmospheric lifetimes, Journal of Physical Chemistry A, 108, 1973–1979, https://doi.org/10.1021/jp0373088, 2004.

Hurley, M. D., Ball, J. C., Wallington, T. J., Sulbaek Andersen, M. P., Nielsen, C. J., Ellis, D. A., Martin, J. W., and Mabury, S. A.: Atmospheric chemistry of n-$C_xF_{2x+1}CHO$ (x = 1,2,3,4): Fate of n-$C_xF_{2x+1}C(O)$ radicals, Journal of Physical Chemistry A, 110, 12443–12447, 2006.

Jiménez, E., González, S., Cazaunau, M., Chen, H., Ballesteros, B., Daële, V., Albaladejo, J., and Mellouki, A.: Atmospheric Degradation Initiated by OH Radicals of the Potential Foam Expansion Agent, $CF_3(CF_2)_2CH{=}CH_2$ (HFC-1447fz): Kinetics and Formation of Gaseous Products and Secondary Organic Aerosols, Environmental Science and Technology, 50, 1234–1242, https://doi.org/10.1021/acs.est.5b04379, 2016.

Kállay, M., Nagy, P. R., Mester, D., Rolik, Z., Samu, G., Csontos, J., Csóka, J., Szabó, P. B., Gyevi-Nagy, L., Hégely, B., Ladjánszki, I., Szegedy, L., Ladóczki, B., Petrov, K., Farkas, M., Mezei, P. D., and Ganyecz, Á.: The MRCC program system: Accurate quantum chemistry from water to proteins., The Journal of chemical physics, 152, 74107, https://doi.org/10.1063/1.5142048, 2020.

Kállay, M., Nagy, P. R., Mester, D., Gyevi-Nagy, L., Csóka, J., Szabó, P. B., Rolik, Z., Samu, G., Csontos, J., Hégely, B., Ganyecz, Á., Ladjánszki, I., Szegedy, L., Ladóczki, B., Petrov, K., Farkas, M., and Mezei, P. D.: MRCC, a quantum chemical program suite, https://mrcc.hu/ (last access: 17 October 2025), 2022.

Kenyon, R. L.: The Path of Chemical Reactions — The IRC Approach, Accounts of Chemical Research, 46, 5, https://doi.org/10.1021/cen-v046n004.p005, 1968.

King, M. D., Canosa-Mas, C. E., and Wayne, R. P.: Gas-phase reactions between RO_2 and NO, HO_2 or CH_3O_2: correlations between rate constants and the SOMO energy of the peroxy (RO_2) radical, Atmospheric Environment, 35, 2081–2088, https://doi.org/10.1016/S1352-2310(00)00501-X, 2001.

Knizia, G., Adler, T. B., and Werner, H. J.: Simplified CCSD(T)-F12 methods: Theory and benchmarks, Journal of Chemical Physics, 130, 054104, https://doi.org/10.1063/1.3054300, 2009.

Kuhler, K. M., Truhlar, D. G., and Isaacson, A. D.: General method for removing resonance singularities in quantum mechanical perturbation theory, The Journal of Chemical Physics, 104, 4664–4671, https://doi.org/10.1063/1.471161, 1996.

Lee, B. H., Munger, J. W., Wofsy, S. C., Rizzo, L. V., Yoon, J. Y. S., Turner, A. J., Thornton, J. A., and Swann, A. L. S.: Sensitive Response of Atmospheric Oxidative Capacity to the Uncertainty in the Emissions of Nitric Oxide (NO) From Soils in Amazonia, Geophysical Research Letters, 51, e2023GL107214, https://doi.org/10.1029/2023GL107214, 2024.

Lelieveld, J., Gromov, S., Pozzer, A., and Taraborrelli, D.: Global tropospheric hydroxyl distribution, budget and reactivity, Atmos. Chem. Phys., 16, 12477–12493, https://doi.org/10.5194/acp-16-12477-2016, 2016.

Lew, M. M., Rickly, P. S., Bottorff, B. P., Reidy, E., Sklaveniti, S., Léonardis, T., Locoge, N., Dusanter, S., Kundu, S., Wood, E., and Stevens, P. S.: OH and HO_2 radical chemistry in a midlatitude forest: measurements and model comparisons, Atmos. Chem. Phys., 20, 9209–9230, https://doi.org/10.5194/acp-20-9209-2020, 2020.

Li, K., Guo, Y., Nizkorodov, S. A., Rudich, Y., Angelaki, M., Wang, X., An, T., Perrier, S., and George, C.: Spontaneous dark formation of OH radicals at the interface of aqueous atmospheric droplets, Proceedings of the National Academy of Sciences of the United States of America, 120, e2220228120, https://doi.org/10.1073/pnas.2220228120, 2023.

Li, M., Karu, E., Brenninkmeijer, C., Fischer, H., Lelieveld, J., and Williams, J.: Tropospheric OH and stratospheric OH and Cl concentrations determined from CH_4, CH_3Cl, and SF_6 measurements, npj Climate and Atmospheric Science, 1, 29, https://doi.org/10.1038/s41612-018-0041-9, 2018.

Li, X., Wang, Y., Cui, J., Shi, Y., and Cai, Y.: Occurrence and Fate of Per- and Polyfluoroalkyl Substances (PFAS) in Atmosphere: Size-Dependent Gas-Particle Partitioning, Precipitation Scavenging, and Amplification, Environmental Science and Technology, 58, 9283–9291, https://doi.org/10.1021/acs.est.4c00569, 2024.

Lin, H., Jacob, D. J., Lundgren, E. W., Sulprizio, M. P., Keller, C. A., Fritz, T. M., Eastham, S. D., Emmons, L. K., Campbell, P. C., Baker, B., Saylor, R. D., and Montuoro, R.: Harmonized Emissions Component (HEMCO) 3.0 as a versatile emissions component for atmospheric models: application in the GEOS-Chem, NASA GEOS, WRF-GC, CESM2, NOAA GEFS-Aerosol, and NOAA UFS models, Geosci. Model Dev., 14, 5487–5506, https://doi.org/10.5194/gmd-14-5487-2021, 2021.

Liu, J. Y., Long, Z. W., Mitchell, E., and Long, B.: New Mechanistic Pathways for the Reactions of Formaldehyde with Formic Acid Catalyzed by Sulfuric Acid and Formaldehyde with Sulfuric Acid Catalyzed by Formic Acid: Formation of Potential Secondary Organic Aerosol Precursors, ACS Earth and Space Chemistry, 5, 1363–1372, https://doi.org/10.1021/acsearthspacechem.1c00002, 2021.

Liu, Y. P., Lynch, G. C., Truong, T. N., Lu, D. hong, Truhlar, D. G., and Garrett, B. C.: Molecular Modeling of the Kinetic Isotope Effect for the [1,5] Sigmatropic Rearrangement of cis-1,3-Pentadiene, Journal of the American Chemical Society, 115, 2408–2415, https://doi.org/10.1021/ja00059a041, 1993.

Long, B., Bao, J. L., and Truhlar, D. G.: Atmospheric Chemistry of Criegee Intermediates: Unimolecular Reactions and Reactions with Water, Journal of the American Chemical Society, 138, 14409–14422, https://doi.org/10.1021/jacs.6b08655, 2016.

Long, B., Bao, J. L., and Truhlar, D. G.: Rapid unimolecular reaction of stabilized Criegee intermediates and implications for atmospheric chemistry, Nature Communications, 10, 2003, https://doi.org/10.1038/s41467-019-09948-7, 2019.

Long, B., Xia, Y., and Truhlar, D. G.: Quantitative Kinetics of HO_2 Reactions with Aldehydes in the Atmosphere: High-Order Dynamic Correlation, Anharmonicity, and Falloff Effects Are All Important, Journal of the American Chemical Society, 144, 19910–19920, https://doi.org/10.1021/jacs.2c07994, 2022.

Long, B., Zhang, Y.-Q., Xie, C., Tan, X.-F., and Truhlar, D. G.: Reaction of Carbonyl Oxide with Hydroperoxymethyl Thioformate: Quantitative Kinetics and Atmospheric Implications, Research, 7, 525, https://doi.org/10.34133/research.0525, 2024.

Lynch, B. J., Zhao, Y., and Truhlar, D. G.: Effectiveness of diffuse basis functions for calculating relative energies by density functional theory, Journal of Physical Chemistry A, 107, 1384–1388, https://doi.org/10.1021/jp021590l, 2003.

Martin, J. W., Mabury, S. A., and O'Brien, P. J.: Metabolic products and pathways of fluorotelomer alcohols in isolated rat hepatocytes, Chemico-Biological Interactions, 155, 165–180, https://doi.org/10.1016/j.cbi.2005.06.007, 2005.

McDuffie, E. E., Smith, S. J., O'Rourke, P., Tibrewal, K., Venkataraman, C., Marais, E. A., Zheng, B., Crippa, M., Brauer, M., and Martin, R. V.: A global anthropogenic emission inventory of atmospheric pollutants from sector- and fuel-specific sources (1970–2017): an application of the Community Emissions Data System (CEDS), Earth Syst. Sci. Data, 12, 3413–3442, https://doi.org/10.5194/essd-12-3413-2020, 2020.

Nie, W., Yan, C., Yang, L., Roldin, P., Liu, Y., Vogel, A. L., Molteni, U., Stolzenburg, D., Finkenzeller, H., Amorim, A., Bianchi, F., Curtius, J., Dada, L., Draper, D. C., Duplissy, J., Hansel, A., He, X. C., Hofbauer, V., Jokinen, T., Kim, C., Lehtipalo, K., Nichman, L., Mauldin, R. L., Makhmutov, V., Mentler, B., Mizelli-Ojdanic, A., Petäjä, T., Quéléver, L. L. J., Schallhart, S., Simon, M., Tauber, C., Tomé, A., Volkamer, R., Wagner, A. C., Wagner, R., Wang, M., Ye, P., Li, H., Huang, W., Qi, X., Lou, S., Liu, T., Chi, X., Dommen, J., Baltensperger, U., El Haddad, I., Kirkby, J., Worsnop, D., Kulmala, M., Donahue, N. M., Ehn, M., and Ding, A.: NO at low concentration can enhance the formation of highly oxygenated biogenic molecules in the atmosphere, Nature Communications, 14, 3347, https://doi.org/10.1038/s41467-023-39066-4, 2023.

Orlando, J. J., Iraci, L. T., and Tyndall, G. S.: Chemistry of the cyclopentoxy and cyclohexoxy radicals at subambient temperatures, Journal of Physical Chemistry A, 104, 5072–5079, https://doi.org/10.1021/jp0002648, 2000.

Rand, A. A. and Mabury, S. A.: Is there a human health risk associated with indirect exposure to perfluoroalkyl carboxylates (PFCAs)?, Toxicology, 375, 28–36, https://doi.org/10.1016/j.tox.2016.11.011, 2017.

Rupp, J., Guckert, M., Berger, U., Drost, W., Mader, A., Nödler, K., Nürenberg, G., Schulze, J., Söhlmann, R., and Reemtsma, T.: Comprehensive target analysis and TOP assay of per- and polyfluoroalkyl substances (PFAS) in wild boar livers indicate contamination hot-spots in the environment, Science of the Total Environment, 871, 162028, https://doi.org/10.1016/j.scitotenv.2023.162028, 2023.

Sellevåg, S. R., Kelly, T., Sidebottom, H., and Nielsen, C. J.: A study of the IR and UV-Vis absorption cross-sections, photolysis and OH-initiated oxidation of CF_3CHO and CF_3CH_2CHO, Phys. Chem. Chem. Phys., 6, 1243–1252, https://doi.org/10.1039/B315941H, 2004.

Solignac, G., Mellouki, A., Le Bras, G., Yujing, M., and Sidebottom, H.: The gas phase tropospheric removal of fluoroaldehydes ($C_xF_{2x+1}CHO$, $x = 3, 4, 6$), Physical Chemistry Chemical Physics, 9, 4200–4210, https://doi.org/10.1039/b614502g, 2007.

Stone, D., Whalley, L. K., and Heard, D. E.: Tropospheric OH and HO_2 radicals: Field measurements and model comparisons, Chemical Society Reviews, 41, 6348–6404, https://doi.org/10.1039/c2cs35140d, 2012.

Sulbaek Andersen, M. P., Hurley, M. D., Wallington, T. J., Ball, J. C., Martin, J. W., Ellis, D. A., Mabury, S. A., and Nielsen, O. J.: Atmospheric chemistry of C_2F_5CHO: Reaction with Cl atoms and OH radicals, IR spectrum of $C_2F_5C(O)O_2NO_2$, Chemical Physics Letters, 379, 28–36, https://doi.org/10.1016/j.cplett.2003.08.004, 2003.

Sulbaek Andersen, M. P., Toft, A., Nielsen, O. J., Hurley, M. D., Wallington, T. J., Chishima, H., Tonokura, K., Mabury, S. A., Martin, J. W., and Ellis, D. A.: Atmospheric Chemistry of Perfluorinated Aldehyde Hydrates (n- $C_xF_{2x+1}CH(OH)_2$, $x = 1, 3, 4$): Hydration, Dehydration, and Kinetics and Mechanism of Cl Atom and OH Radical Initiated Oxidation, The Journal of Physical Chemistry A, 110, 9854–9860, https://doi.org/10.1021/jp060404z, 2006.

Sznajder-Katarzyńska, K., Surma, M., and Cieślik, I.: A Review of Perfluoroalkyl Acids (PFAAs) in terms of Sources, Applications, Human Exposure, Dietary Intake, Toxicity, Legal Regulation, and Methods of Determination, Journal of Chemistry, 2019, 2717528, https://doi.org/10.1155/2019/2717528, 2019.

Taube, A. G. and Bartlett, R. J.: Frozen natural orbital coupled-cluster theory: Forces and application to decomposition of nitroethane, Journal of Chemical Physics, 128, 164101, https://doi.org/10.1063/1.2902285, 2008.

Thackray, C. P., Selin, N. E., and Young, C. J.: A global atmospheric chemistry model for the fate and transport of PFCAs and their precursors, Environmental Science: Processes and Impacts, 22, 285–293, https://doi.org/10.1039/c9em00326f, 2020.

Thomson, A. J., Giannopoulos, G., Pretty, J., Baggs, E. M., and Richardson, D. J.: Biological sources and sinks of nitrous oxide and strategies to mitigate emissions, Philosophical Transactions of the Royal Society B, 367, 1157–1168, https://doi.org/10.1098/rstb.2011.0415, 2012.

Thomson, J. D., Campbell, J. S., Edwards, E. B., Medcraft, C., Nauta, K., Pérez-Peña, M. P., Fisher, J. A., Osborn, D. L., Kable, S. H., and Hansen, C. S.: Fluoroform (CHF_3) Production from CF_3CHO Photolysis and Implications for the Decomposition of Hydrofluoroolefins and Hydrochlorofluoroolefins in the Atmosphere, Journal of the American Chemical Society, 147, 33–38, https://doi.org/10.1021/jacs.4c11776, 2025.

Truhlar, D. G., Isaacson, A. D., Skodje, R. T., and Garrett, B. C.: Incorporation of quantum effects in generalized-transition-state theory, Journal of Physical Chemistry, 86, 2252–2261, https://doi.org/10.1021/j100209a021, 1982.

Vereecken, L. and Peeters, J.: Decomposition of substituted alkoxy radicals – Part I: A generalized structure-activity relationship for reaction barrier heights, Physical Chemistry Chemical Physics, 11, 9062–9074, https://doi.org/10.1039/b909712k, 2009.

Wang, Y., Liu, J., Yang, L., Zhao, X., Ji, Y. M., and Li, Z.: Theoretical studies and rate constant calculations of the reactions C_2F_5CHO with OH radicals and Cl atoms, Journal of Molecular Structure: THEOCHEM, 820, 26–34, https://doi.org/10.1016/j.theochem.2007.06.001, 2007.

Wang, X., Jacob, D. J., Eastham, S. D., Sulprizio, M. P., Zhu, L., Chen, Q., Alexander, B., Sherwen, T., Evans, M. J., Lee, B. H., Haskins, J. D., Lopez-Hilfiker, F. D., Thornton, J. A., Huey, G. L., and Liao, H.: The role of chlorine in global

tropospheric chemistry, Atmos. Chem. Phys., 19, 3981–4003, https://doi.org/10.5194/acp-19-3981-2019, 2019.

Wang, Y., Wang, Z., Sun, M., Guo, J., and Zhang, J.: Emissions, degradation and impact of HFO-1234ze from China PU foam industry, Science of the Total Environment, 780, 146631, https://doi.org/10.1016/j.scitotenv.2021.146631, 2021.

Wang, Y., Liu, L., Qiao, X., Sun, M., Guo, J., Zhang, J., and Zhao, B.: Projections of National-Gridded Emissions of Hydrofluoroolefins (HFOs) in China, Environmental Science and Technology, 57, 8650–8659, https://doi.org/10.1021/acs.est.2c09263, 2023.

Wang, Y., Liu, L., Qiao, X., Sun, M., Guo, J., Zhao, B., and Zhang, J.: Atmospheric fate and impacts of HFO-1234yf from mobile air conditioners in East Asia, Science of the Total Environment, 916, 170137, https://doi.org/10.1016/j.scitotenv.2024.170137, 2024.

Waterland, R. L. and Dobbs, K. D.: Atmospheric chemistry of linear perfluorinated aldehydes: Dissociation kinetics of $C_nF_{2n+1}CO$ radicals, Journal of Physical Chemistry A, 111, 2555–2562, https://doi.org/10.1021/jp067587+, 2007.

Werner, H.-J., Knowles, P. J., Knizia, G., Manby, F. R., Schütz, M., Celani, P., Györffy, W., Kats, D., Korona, T., Lindh, R., Mitrushenkov, A., Rauhut, G., Shamasundar, K. R., Adler, T. B., Amos, R. D., Bennie, S. J., Bernhardsson, A., Berning, A., Cooper, D. L., Deegan, M. J. O., Dobbyn, A. J., Eckert, F., Goll, E., Hampel, C., Hesselmann, A., Hetzer, G., Hrenar, T., Jansen, G., Köppl, C., Lee, S. J. R., Liu, Y., Lloyd, A. W., Ma, Q., Mata, R. A., May, A. J., McNicholas, S. J., Meyer, W., Miller III, T. F., Mura, M. E., Nicklass, A., O'Neill, D. P., Palmieri, P., Peng, D., Pflüger, K., Pitzer, R., Reiher, M., Shiozaki, T., Stoll, H., Stone, A. J., Tarroni, R., Thorsteinsson, T., Wang, M., and Welborn, M.: MOLPRO, version 2019.2, a package of ab initio programs, https://www.molpro.net/ (last access: 17 October 2025), 2019.

Wu, J., Zhuang, Y., Dong, B., Wang, F., Yan, Y., Zhang, D., Liu, Z., Duan, X., Bo, Y., and Peng, L.: Spatial heterogeneity of per- and polyfluoroalkyl substances caused by glacial melting in Tibetan Lake Nam Co due to global warming, Journal of Hazardous Materials, 478, 135468, https://doi.org/10.1016/j.jhazmat.2024.135468, 2024.

Xia, Y., Long, B., Liu, A., and Truhlar, D. G.: Reactions with criegee intermediates are the dominant gas-phase sink for formyl fluoride in the atmosphere, Fundamental Research, 4, 1216–1224, https://doi.org/10.1016/j.fmre.2023.02.012, 2024a.

Xia, D., Zhang, H., Ju, Y., Xie, H., Su, L., Ma, F., Jiang, J., Chen, J., and Francisco, J. S.: Spontaneous Degradation of the "Forever Chemicals" Perfluoroalkyl and Polyfluoroalkyl Substances (PFASs) on Water Droplet Surfaces, Journal of the American Chemical Society, 146, 11266–11271, https://doi.org/10.1021/jacs.4c00435, 2024b.

Yang, X., Wang, Q., Ma, N., Hu, W., Gao, Y., Huang, Z., Zheng, J., Yuan, B., Yang, N., Tao, J., Hong, J., Cheng, Y., and Su, H.: The impact of chlorine chemistry combined with heterogeneous N_2O_5 reactions on air quality in China, Atmos. Chem. Phys., 22, 3743–3762, https://doi.org/10.5194/acp-22-3743-2022, 2022.

Yu, T., Zheng, J., and Truhlar, D. G.: Multipath variational transition state theory: Rate constant of the 1,4-hydrogen shift isomerization of the 2-cyclohexylethyl radical, Journal of Physical Chemistry A, 116, 297–308, https://doi.org/10.1021/jp209146b, 2012.

Yu, Y., Pan, L., Sun, Q., and Wang, J.: The mechanism and kinetics of the atmospheric oxidation of $CF_3(CF_2)_2CH = CH_2$ (HFC-1447fz) by hydroxyl radicals: ab initio investigation, Physical Chemistry Chemical Physics, 26, 10989–10997, https://doi.org/10.1039/d3cp06149c, 2024.

Zhang, T., Zhang, Y., Wen, M., Tang, Z., Long, B., Yu, X., Zhao, C., and Wang, W.: Effects of water, ammonia and formic acid on $HO_2 + Cl$ reactions under atmospheric conditions: Competition between a stepwise route and one elementary step, RSC Advances, 9, 21544–21556, https://doi.org/10.1039/c9ra03541a, 2019.

Zhang, W., Issa, K., Tang, T., and Zhang, H.: Role of Hydroperoxyl Radicals in Heterogeneous Oxidation of Oxygenated Organic Aerosols, Environmental Science and Technology, 58, 4727–4736, https://doi.org/10.1021/acs.est.3c09024, 2024.

Zhang, Y., Cheng, Y., Zhang, T., Wang, R., Ji, J., Xia, Y., Lily, M., Wang, Z., and Muthiah, B.: A computational study of the $HO_2 + SO_3 \rightarrow HOSO_2 + 3O_2$ reaction catalyzed by a water monomer, a water dimer and small clusters of sulfuric acid: kinetics and atmospheric implications, Physical Chemistry Chemical Physics, 24, 18205–18216, https://doi.org/10.1039/d1cp03318b, 2022.

Zhao, Y. and Truhlar, D. G.: Exploring the limit of accuracy of the global hybrid meta density functional for main-group thermochemistry, kinetics, and noncovalent interactions, Journal of Chemical Theory and Computation, 4, 1849–1868, https://doi.org/10.1021/ct800246v, 2008a.

Zhao, Y. and Truhlar, D. G.: The M06 suite of density functionals for main group thermochemistry, thermochemical kinetics, noncovalent interactions, excited states, and transition elements: Two new functionals and systematic testing of four M06 functionals and 12 other functionals, Theoretical Chemistry Accounts, 120, 215–241, https://doi.org/10.1007/s00214-007-0401-8, 2008b.

Zheng, J. and Truhlar, D. G.: Kinetics of hydrogen-transfer isomerizations of butoxyl radicals, Physical Chemistry Chemical Physics, 12, 7782–7793, https://doi.org/10.1039/b927504e, 2010.

Zheng, J. and Truhlar, D. G.: Quantum thermochemistry: Multistructural method with torsional anharmonicity based on a coupled torsional potential, Journal of Chemical Theory and Computation, 9, 1356–1367, https://doi.org/10.1021/ct3010722, 2013.

Zheng, J., Yu, T., Papajak, E., Alecu, I. M., Mielke, S. L., and Truhlar, D. G.: Practical methods for including torsional anharmonicity in thermochemical calculations on complex molecules: The internal-coordinate multi-structural approximation, Physical Chemistry Chemical Physics, 13, 10885–10907, https://doi.org/10.1039/c0cp02644a, 2011.

Zheng, J., Meana-Pañeda, R., and Truhlar, D. G.: Prediction of Experimentally Unavailable Product Branching Ratios for Biofuel Combustion: The Role of Anharmonicity in the Reaction of Isobutanol with OH, Journal of the American Chemical Society, 136, 5150–5160, https://doi.org/10.1021/ja5011288, 2014.

Zheng, J., Oyedepo, G. A., and Truhlar, D. G.: Kinetics of the Hydrogen Abstraction Reaction From 2-Butanol by OH Radical, The Journal of Physical Chemistry A, 119, 12182–12192, https://doi.org/10.1021/acs.jpca.5b06121, 2015.

Zheng, J., Bao, J. L., Meana-Pañeda, R., Zhang, S., J.Lynch, B., Corchado, J. C., Chuang, Y., Fast, P. L., Hu, W.-P., Liu, Y.-P., Lynch, G. C., Nguyen, K. A., Jackels, C. F., Ramos, A. F., Elling-

son, B. A., Melissas, V. S., Villà, J., Rossi, I., Coitiño, E. L., Pu, J., Albu, T. V., Ratkiewicz, A., Steckler, R., Garrett, B. C., Isaacson, A. D., and Truhlar, D. G.: Polyrate-version 2017-C; University of Minnesota: Minneapolis, 2017.

Zheng, J., Bao, J. L., Zhang, S., Corchado, J. C., Chuang, Y., Ellingson, B. A., and Truhlar, D. G.: Gaussrate, version 2017-B; University of Minnesota: Minneapolis, MN, https://comp.chem.umn.edu/polyrate/ (last access: 17 October 2025), 2018.

Zhou, J., Fukusaki, Y., Murano, K., Gautam, T., Bai, Y., Inomata, Y., Komatsu, H., Takeda, M., Yuan, B., Shao, M., Sakamoto, Y., and Kajii, Y.: Investigation of HO_2 uptake mechanisms onto multiple-component ambient aerosols collected in summer and winter time in Yokohama, Japan, Journal of Environmental Sciences (China), 137, 18–29, https://doi.org/10.1016/j.jes.2023.02.030, 2024a.

Zhou, Y., Wang, X., Wang, C., Ji, Z., Niu, X., and Dong, H.: Fate of 'forever chemicals' in the global cryosphere, Earth-Science Reviews, 259, 104973, https://doi.org/10.1016/j.earscirev.2024.104973, 2024b.

Ziemann, P. J. and Atkinson, R.: Kinetics, products, and mechanisms of secondary organic aerosol formation, Chemical Society Reviews, 41, 6582–6605, https://doi.org/10.1039/c2cs35122f, 2012.